Journal of Geophysical Research: Oceans
DOI 10.1002/2015JC011599

Carbon exchange between a shelf sea and the ocean: The Hebrides Shelf, west of Scotland

Stuart C. Painter[1*], Susan E. Hartman[1], Caroline Kivimäe[1], Lesley A. Salt[2], Nicola M. Clargo[3], Yann Bozec[2], Chris J. Daniels[1], Sam C. Jones[4,5], Victoria S. Hemsley[1,6], Lucie R. Munns[1,6], Stephanie R. Allen[1,6]

[1]National Oceanography Centre, European Way, Southampton, SO14 3ZH, UK

[2]Sorbonnes Universités, UPMC Univ Paris 06, CNRS, UMR 7144 Adaptation et Diversité en Milieu Marin, Station Biologique de Roscoff, Place Georges Teissier, 29680 Roscoff, France

[3]Royal Netherlands Institute for Sea Research, P.O. Box 59, 1790 AB Den Burg, Texel, the Netherlands.

[4]Scottish Association for Marine Science (SAMS), Oban, PA37 1QA, UK

[5] Department of Physics, University of Aberdeen, Aberdeen, AB24 3FX, UK

[6]Ocean and Earth Science, University of Southampton, National Oceanography Centre, European Way, Southampton SO14 3ZH, UK

Resubmitted 16/05/2016

Journal of Geophysical Research - Oceans

*corresponding author

National Oceanography Centre, European Way, Southampton, SO14 3ZH, UK

Tel: +44 (0) 23 8059 6209

Fax: +44 (0) 23 8059 6247

Email: stuart.painter@noc.ac.uk

Received: Dec 22, 2015; Revised: May 16, 2016; Accepted: May 21, 2016

Highlights

Cross-shelf transports and carbon fluxes are reported for the Hebrides Shelf.

The mean Ekman drain downslope transport was 1.81 $m^2 s^{-1}$, but important 4-fold spatial variability was identified.

The Hebrides Shelf may export 5-times more POC per unit area via the Ekman drain than the global mean

Abstract

Global mass balance calculations indicate the majority of particulate organic carbon (POC) exported from shelf seas is transferred via downslope exchange processes. Here we demonstrate the downslope flux of POC from the Hebrides Shelf is approximately 3-to-5-fold larger per unit length/area than the global mean. To reach this conclusion we quantified the offshore transport of particulate and dissolved carbon fractions via the "Ekman Drain", a strong downwelling feature of the NW European Shelf circulation, and subsequently compared these fluxes to simultaneous regional air-sea CO_2 fluxes and on-shore wind-driven Ekman fluxes to constrain the carbon dynamics of this shelf. Along the shelf break we estimate a mean offshelf total carbon (dissolved + particulate) flux of 4.2 tonnes C m^{-1} d^{-1} compared to an onshelf flux of 4.5 tonnes C m^{-1} d^{-1}. Organic carbon represented 3.3% of the onshelf carbon flux but 6.4% of the offshelf flux indicating net organic carbon export. Dissolved organic carbon represented 95% and POC 5% of the exported organic carbon pool. When scaled along the shelf break the total offshelf POC flux (0.007 Tg C d^{-1}) was found to be three times larger than the regional air-sea CO_2 ingassing flux (0.0021 Tg C d^{-1}), an order of magnitude larger than the particulate inorganic carbon flux (0.0003 Tg C d^{-1}) but far smaller than the DIC (2.03 Tg C d^{-1}) or DOC (0.13 Tg C d^{-1}) fluxes. Significant spatial heterogeneity in the Ekman drain transport confirms that offshelf carbon fluxes via this mechanism are also spatially heterogeneous.

1. Introduction

The temperate coastal ocean is an important sink for atmospheric CO_2 but changing environmental conditions are likely to alter the effectiveness of this sink in future (Bauer *et al.,* 2013; Regnier *et al.,* 2013). Initial estimates extrapolated from the East China Sea suggested the global coastal ocean absorbed almost 1 Pg C yr^{-1} (Tsunogai *et al.,* 1999). Continued improvement in observational capability, data synthesis activities and analytical methodologies however has resulted in a progressive decrease in the magnitude of this sink term (see summary in Chen *et al.*, 2013) with one recent estimate suggesting a global carbon sink in coastal seas of ~0.2 Pg C yr^{-1} (Laruelle *et al.,* 2014). Despite efforts to improve estimates of the global CO_2 sink in coastal seas there is still considerable uncertainty in the contribution of individual shelf seas to regional carbon budgets, a situation that precludes accurate prediction of future events (Borges 2005).

The Northwest European Shelf is one of the best-studied continental shelf regions in the world with data coverage that is considered sufficient to allow calculation of seasonal air-sea CO_2 fluxes with high confidence (Thomas *et al.,* 2004; Chen *et al.,* 2013; Laruelle *et al.,* 2014). The Hebrides Shelf, to the west of Scotland, makes up the north-western extremity of the NW European Shelf and accounts for ~7% of the total area of the NW European Shelf. It is however a region of significant exchange of water with the open ocean with models and long-term observations suggesting typical onshore wind driven exchanges and compensating downwelling offshelf fluxes of ~1 Sv (Holt *et al.,* 2009; Huthnance *et al.,* 2009; Huthnance 2010; Wakelin *et al.,* 2012). The strong downwelling circulation along the Hebrides Shelf edge, and more widely along the NW European Shelf edge, is considered a vital conduit for the export of

carbon to the open ocean but it remains poorly constrained observationally (Holt *et al.,* 2009; Huthnance *et al.,* 2009; Wakelin *et al.,* 2012; Simpson and McCandliss 2013).

The downwelling circulation is induced by the European Slope Current, a warm and saline northerly flowing current located over the upper continental slope of the NW European shelf that is considered an important route for the transfer of heat and salt to the Arctic, and which in winter, likely runs continuously from the Bay of Biscay to the Norwegian Sea (Huthnance 1986; Pingree 1993; Xu *et al.,* 2015). The Slope Current is typically centred above the 500 m bathymetric contour, generally below the seasonal thermocline, and closely follows the bathymetry northwards (Booth and Ellett 1983). Measurements within the Slope Current indicate typical current velocities of 0.2-0.4 m s^{-1}, and transports of ~1.5 Sv, though there is considerable variability with latitude and by season with increased current velocities and transports northwards and throughout autumn and winter (Dickson *et al.,* 1986; Huthnance 1986; Carter *et al.,* 1987; Xu *et al.,* 2015). Over the inner shelf, and predominately inshore of the Hebridean Islands, runs the Scottish Coastal Current, another northward flowing current, with a mean velocity of ~0.11 m s^{-1} and a volume transport of ~0.1 Sv (McKay *et al.,* 1986; Inall *et al.,* 2009). In addition to distinct currents a residual northward flow exists over the wider Hebrides Shelf (McKay *et al.,* 1986; Xing and Davies 1996). Near-geostrophy within the Slope Current greatly restricts direct cross-shelf exchange with the open ocean and long-term observations indicate typical cross shelf current velocities of <0.04 m s^{-1} (Booth and Ellett 1983; Huthnance 1986; Souza *et al.,* 2001; Simpson and McCandliss 2013). However, a strong cross-shelf downwelling circulation is induced under the Slope Current via frictional stresses

within the bottom boundary layer overcoming geostrophic control. This process, known as the "Ekman Drain", can result in significant offshelf transport close to the seabed. Limited observational evidence suggests a particulate carbon flux of 30 kmols C m^{-1} yr^{-1} (0.36 tonnes C m^{-1} yr^{-1}) associated with the Ekman drain along the Hebrides Shelf (Simpson and McCandliss 2013). Model estimates however differ markedly with the modelled flux of 23-41 kmol C m^{-1} yr^{-1} obtained by Proctor *et al*., (2003) being far smaller than the total organic carbon flux of 180 kmol C m^{-1} yr^{-1} derived from the model results of Wakelin *et al*., (2012), indicating that additional observational constraints of the various carbon pools and fluxes are needed.

In this study we simultaneously estimate the cross shelf downwelling transport, the wind-driven surface Ekman transport, the associated fluxes of carbon and the air-sea CO_2 flux from new observations on the Hebrides Shelf to determine the significance of all terms to a regional carbon budget.

2. Methods

During October and November 2014 six cross-shelf transects were undertaken between 55.3°N and ~59.2°N (**Figure 1**). A total of 56 full-depth CTD casts were conducted at 37 stations with water samples collected from 5 to 24 depths at each station. Water column depths ranged from 75 to ~2100 m and transect lengths varied from ~80 to ~140 km with an average along-track station spacing of 24 km. Bad weather prevented the completion of transect B.

Marine Scotland designate seven 'sea regions' around Scotland for statutory purposes which includes the Hebrides Sea Region, a formally designated area of 41,134 km^2

stretching westwards from the west coast of the Hebrides Islands to the 1000 m bathymetric contour and from ~56°N to ~59°N (Baxter *et al.,* 2011). This region is smaller than that sampled during the cruise (**Figure 1**) so to formulate regional fluxes utilising all available data we extended the geographical limits of this sea region to the northern and southern extremities of our data (~55.3°N to 59.2°N) whilst maintaining the 1000 m contour as the western boundary and the nominal inshore eastern boundary at 7.8°W (**Figure 1**). This new extended region covers ~54,747 km^2, and represents approximately 5% of the total area of the NW European Shelf (1112 x 10^3 km^2).

Nutrients

Concentrations of nitrate (NO_3+NO_2; hereafter nitrate), phosphate (PO_4^{3-}), and silicic acid (Si(OH)4; hereafter silicate) were measured on discrete water samples collected via CTD/rosette sampling. Water samples were collected from all sampled depths direct from CTD Niskin bottles into 25 ml plastic vials and analysed immediately or refrigerated at 4°C until analysis. All samples were analysed on a Skalar Sanplus autoanlyser using common methodologies (e.g. Kirkwood et al., 1996; Hydes et al., 2010).

Dissolved Inorganic Carbon and Total Alkalinity

Dissolved inorganic carbon (DIC) and total alkalinity (T_A) were sampled and measured according to best practice procedures (Dickson *et al.,* 2007). 0.6 litre water samples were collected from the CTD Niskin bottles at all sampled depths and stations into borosilicate glass bottles with plastic caps using tygon tubing. Analysis commenced immediately after sampling in a temperature controlled laboratory using

two VINDTA 3C instruments. A fresh bottle of certified reference material (CRM, Batch 140) was used to ensure accuracy for each station and all analyses were completed within 12 hours of sampling. The analytical precision based on replicate CRM analysis was ±2.2 μmol kg^{-1} for alkalinity and ±2.07 μmol kg^{-1} for DIC.

Vessel Mounted Acoustic Doppler Current Profiler (VMADCP)

RRS *Discovery* is fitted with 75 and 150 kHz RDI 'Ocean Surveyor' Acoustic Doppler Current profilers (ADCP). We preferentially used the 75 kHz instrument due to its deeper acoustic penetration and during the cruise this was set to operate in 'narrowband' mode and to average over 120 second intervals with 60 depth bins of 16 m thickness with data acquisition via VM-DAS. Preliminary data processing at sea corrected for instrument mis-alignment angle and vessel motion as described in best-practice guidelines (Firing and Hummon 2010). Technical problems with the operation of the instrument whilst at sea however resulted in intermittent 3- and 4-beam solutions, with the problem eventually traced to a faulty deck-unit, which was swapped mid-cruise resulting in consistent 4-beam solutions thereafter. Consequently usable data only exist for part of transect C and along transects D-G. Data from the 150 kHz instrument are used to provide current information along transect A.

Inspection of the data after the cruise identified several additional problems with data coverage and beam penetration into the water column so the entire dataset was reprocessed using the Python based 'CODAS processing' routines developed by the University of Hawaii (http://currents.soest.hawaii.edu/docs/adcp_doc/index.html). The reprocessing of the data resulted in the production of a dataset with a 10 m

vertical bin resolution and a 15-minute averaging period (5 m vertical resolution for the 150 kHz data).

The VM-ADCP data were detided to remove barotropic tidal oscillations using Oregon State University's Ocean Topography Experiment/Poseidon Cross Over Global Inverse Solution (Egbert *et al.,* 1994; Egbert and Erofeeva 2002) using a 1/30th degree resolution tidal model of the northwest European Shelf (Egbert *et al.,* 2010; model available at http://volkov.oce.orst.edu/tides/) and a Matlab based toolbox to access and extract the tidal components (http://polaris.esr.org/ptm_index.html).

Hydrography

CTD salinity measurements were calibrated against water samples analysed using a Guildline Autosal salinometer and IAPSO seawater standards (P-series). All hydrographic parameters are reported using the new Thermodynamic Equation of State (TEOS-10) terminology (*i.e.* Conservative Temperature (Θ; □□□□□□°C) and Absolute Salinity (S_A; units g kg^{-1}), (IOC SCOR and IAPSO 2010)).

Dissolved Oxygen

Dissolved oxygen concentrations were measured in duplicate using the Winkler whole bottle technique (Langdon 2010). Up to 12 depths on each CTD cast were sampled. The accuracy of the measurements based on duplicate samples was estimated at ±0.3 μmol kg^{-1}. Discrete oxygen measurements were used to calibrate the Seabird-43 dissolved oxygen sensor attached to the CTD rosette frame according to Uchida *et al*., (2010).

Particulate Material

Several classes of particulate material were sampled for during the cruise. These included particulate organic carbon (POC) and particulate organic nitrogen (PON). Concentrations of both were measured on 1-litre seawater samples filtered on to pre-ashed (>450^{o}C for >4 hrs) 25 mm glass fibre filters (Whatman GF/F). After filtration samples were twice rinsed with a weak 1% solution of HCL to remove inorganic carbon. Filters were oven dried at 40^{o}C before being pelleted into tin capsules and analysed for carbon and nitrogen content using a Costech ECS 4010 CHN elemental analyzer.

Particulate organic phosphate (POP) concentrations were measured using the method described by Raimbault *et al*., (1999). Briefly, 1 litre seawater samples were filtered onto pre-combusted, acid washed (10% HCl) GF/F filters, oven dried and stored in sealed pre-combusted glass test tubes until analysis. In the laboratory each filter was transferred to a pyrex screw top test tube (HDPE screwcap with Teflon liner) and a sodium tetraborate/potassium peroxodisulphate oxidising reagent added. Each tube was tightly sealed and placed in an autoclave at 121°C for 30 minutes. Thereafter the sample was centrifuged at 3000 rpm for 30 minutes before the phosphate content was measured by autoanalyser. Oxidation efficiency was assessed via parallel oxidation of an organic reference standard (NIST reference material 1573a, 'Tomato Leaves'). Oxidation efficiency ranged from 79-85%. Consequently, sample POP content was increased by an amount based on the average oxidation efficiency for each batch of samples analysed.

Biogenic silica (bSi) concentrations were measured using the method of Ragueneau and Treguer (1994). Briefly, a 0.5 litre sample was filtered onto a 25 mm diameter 0.8 μm polycarbonate filter, which was dried at 40°C and stored in 15 ml Falcon tubes until akaline digestion and analysis for the Si content could be undertaken. In the laboratory, 5 ml of 0.2M NaOH was added to each Falcon tube to digest the sample, which was baked at 85°C for at least 2 hours. After returning to room temperature approximately 10 ml of 0.1M HCl was added to neutralize the pH of the digested sampled to pH 7-8. The solution was then analysed by autoanalyser as described above for Si analysis. Note that results are reported both as the measured molar concentration of $Si(OH)_4$ when describing typical bSi distributions or are converted to mass of opal assuming a molecular formula of $SiO_2.0.4\ H_2O$ when describing cross-shelf fluxes. Analytical blanks (fresh filters washed with 0.2 μm filtered seawater) were treated as above.

Particulate inorganic carbon (PIC) concentrations were typically measured on a surface sample only and on 0.5 litre seawater samples filtered on to 25 mm 0.2 μm polycarbonate filters. Each filter was rinsed with a weak solution of analytical grade ammonium solution (pH ~9.7) to remove residual sea salt and placed in a 2 ml Eppendorf tube. Filters were oven dried at 40°C and stored until analysis. In the laboratory all samples were weighed, extracted in 3% nitric acid and analysed using Inductively Coupled Plasma Atomic Mass Spectrometry (Green *et al.,* 2003). Sample carbon content (as PIC) was calculated assuming a 1:1 molar equivalency with the measured calcium content (present as $CaCO_3$) of the sample (Van Bleijswijk *et al.,* 1994).

Exchange Rate Calculations

Air-sea flux of CO_2

Estimates of the air-sea CO_2 flux were calculated using a common bulk methodology (e.g. Laruelle *et al.,* 2014). At each station the instantaneous flux of CO_2 was calculated as

$$Flux\ CO_2 = k\ \cdot K'_0\ \cdot \Delta pCO_2 \qquad [1]$$

where k is the gas transfer velocity (m s^{-1}), K'_0 is the CO_2 gas saturation constant calculated from Weiss (1974) using appropriate temperature (in °K) and salinity measurements, and ΔpCO_2 is the difference in partial pressure between seawater and the atmosphere.

The gas transfer velocity was calculated from

$$k = \tau C U^2 \left(\frac{Sc}{660}\right)^{-1/2} \qquad [2]$$

where τ is the transfer coefficient (0.26) of Takahashi et al., (2009), U is the wind speed 10 m above the sea surface, C is a correction factor suggested by Jiang et al., (2008), and Sc is the Schmidt number formulated according to Wanninkhof (1992)

$$Sc = 2073.1 - 125.62\ \cdot SST + 3.6276\ \cdot SST^2 - 0.043219\ \cdot\ SST^3 \qquad [3]$$

where SST is taken from the in-situ measurements.

Due to the failure of the ship fitted meteorological instrument suite we have taken wind speed estimates from the ECMWF global reanalysis product (ERA-Interim), which provides 6 hourly estimates of wind speed on a global 0.75 x 0.75 deg grid.

Wind speeds were linearly interpolated from the ERA-Interim product to the time and position of the sampled stations. Use of this data product necessitated subsequent use of the correction factor (C) suggested by Jiang et al., (2008) to account for nonlinearity between wind speed and gas transfer relationships

$$C = \frac{\frac{1}{n}\sum_j^n U_j^2}{U_{mean}^2} \quad [4]$$

where U_j is the 6 hourly wind speed estimate, and U_{mean} is the mean wind speed over the study period.

Atmospheric pCO_2 was calculated as

$$(pCO_2)_{air} = XCO_2 \cdot (P_{baro} - P_{sw}) \quad [5]$$

where XCO_2 is the mean CO_2 concentration for dry air for October and November 2014 (396.935 ppm) taken from the NOAA global CO_2 record (http://www.esrl.noaa.gov/gmd/ccgg/trends/global.html#global), P_{baro} is barometric pressure at the sea surface interpolated to the time and location of sampling and taken from NCEP-II reanalysis products (Kanamitsu *et al.,* 2002); a global 6 hourly product on a 2.5 x 2.5 deg resolution grid, and Psw is the water vapour pressure at the in-situ temperature and salinity calculated according to Weiss and Price (1980).

We calculated estimates of $(pCO_2)_{sw}$ corrected to in-situ sampling temperatures from the Excel based version of CO_2SYS described by Pelletier *et al.*, (2007) (version 25b06), using the measured DIC and alkalinity as input and using recommended constants throughout (Dickson *et al.,* 2007; Orr *et al.,* 2015).

Finally, we calculated the difference in partial pressure between seawater and the atmosphere as

$$\Delta pCO_2 = (pCO_2)sw - (pCO_2)air \quad [6]$$

In addition to daily flux estimates obtained for each station we also calculated a large area daily integral of CO_2 flux based on the mean station flux and the extended Hebrides Sea Region defined above. This spatial area encompassed 78% of the available data with the remaining 22% of observations located over deep waters off shelf.

Shelf-Edge Exchange and the Flux of Biogenic Material

Cross shelf exchange via the Ekman drain was estimated following the theoretical arguments presented by Souza *et al.,* (2001) and Simpson and McCandliss (2013) which relate barotropic current velocities to down-slope cross-shelf exchange via the equation

$$Tb = \frac{K_b \bar{V}^2}{f} \quad [7]$$

where *Tb* is the down-slope transport in the bottom Ekman Layer (units $m^2\ s^{-1}$), *Kb* is the bottom drag coefficient (0.0025, unitless), $\bar{V}$ is the depth averaged current ($m\ s^{-1}$), and *f* the Coriolis parameter. Where possible we calculated the maximum depth averaged meridional current (*V*) for each transect corresponding to the core of the Slope Current from the detided VM-ADCP data. The exception being transect A where, due to the rotation of the current around the continental shelf bathymetry, we used the zonal current (*U*). This was then used as input to equation 7 to estimate the

down-slope transport for each transect (units of m^2 s^{-1}). Shelf wide horizontal volume transports (m^3 s^{-1}) were subsequently calculated by multiplying the transport estimate from each transect by the length of the slope (516 km; determined as the distance along the 200 m bathymetric contour between the southernmost and northernmost transects). This resulted in six separate estimates of shelf wide volume transport.

To estimate the associated flux of biogenic material to the open ocean via the Ekman drain we considered two different approaches. In the first simpler approach particulate pool concentrations near the seabed at each shelf break station were identified. This provided particulate pool concentrations over a depth range of 187-224 m (in water depths of 195-237 m), comparable to the depth range that the Ekman drain is considered to operate over (Huthnance *et al.,* 2009; Wakelin *et al.,* 2012), but with limited information regarding lateral gradients. In the second approach we calculated a mean concentration for each transect using the deepest samples for shelf and shelf break stations only. This included samples collected over a depth range of 60-224 m and whilst revealing important heterogeneity in particulate distributions near the seabed, with higher concentrations eastwards onto the shelf, may bias upwards the representative concentration entrained into the Ekman drain. Surprisingly, despite differences in particulate concentrations of up to ±30% between the two approaches on each transect (i.e. shelf break vs transect average concentrations could differ by up to ±30%), only modest differences in the overall shelf wide mean particulate concentrations were found suggesting that mean regional fluxes from either method will give comparable results. For example, the mean POC concentration at shelf break stations was 89 mg m^{-3} compared to a mean of 86 mg m^{-3} for all shelf and shelf break stations. Nevertheless, due to the lateral variability in particulate concentration along

each transect and the sensitivity in the calculation of material flux to that variability we have used the shelf break stations only in our calculations. Consequently, near seabed concentrations of POC, PON, POP, and bSi-opal at the shelf break were multiplied by the transport calculated for each transect to obtain the downslope fluxes of material associated with each transect. A similar approach was followed for dissolved constituents. Where stated, the total offshelf export for the Hebrides Shelf is based on the overall mean flux (i.e. the mean of all transect fluxes) and typically reported in units of weight per metre of shelf edge per day (e.g. tonnes C m^{-1} d^{-1}). Exceptions to this occur when extrapolations of individual fluxes along the shelf break are undertaken to estimate the total offshelf flux for the region studied. We have avoided, where possible, the extrapolation of daily fluxes to an annual basis due to an absence of seasonal information on the variability in the slope current and in particulate/dissolved concentrations.

Estimates of the surface wind-driven Ekman flux (T_E) were calculated for comparison to the Ekman drainage flux following Huthnance et al., (2009) using ERA-Interim wind speeds and directions; specifically

$$T_E = \rho_a C_D (W^2 \cos\theta + w'^2) / (\rho_w f) \qquad [8]$$

where ρ_a = 1.25 and ρ_w = 1027 are the densities (kg m^{-3}) of air and seawater, C_D = 0.0012 is the drag coefficient, W is the monthly mean wind speed calculated for the period Oct 15th to Nov 15th 2014, θ is the angle of the wind relative to the orientation of the shelf, w' is the standard deviation of the wind speed in the along slope direction and f is the coriolis parameter. Onshore carbon fluxes were calculated in a similar

manner to the Ekman drain fluxes except for the use of mean mixed layer concentrations as determined from offshore stations.

3. Results

Surface Fields

Strong lateral gradients were seen in surface waters between the shelf and the open ocean (**Figure 2**). Among the most striking were the differences in temperature and absolute salinity with shelf waters being warmer (>12.5°C) and fresher (~<35.3 g kg^{-1}) than surface waters offshore, which were cooler (<12.5 °C) and more saline (>35.5 g kg^{-1}). A notable gradient in dissolved oxygen concentrations was also evident with lower concentrations on the shelf.

Nutrient concentrations were patchily distributed and variable. Nitrate concentrations were typically 2-4 μmol L^{-1} on shelf and reached a maximum concentration of >6 μmol L^{-1} off shelf at station C7, the most northwesterly station sampled. In general, nitrate concentrations increased from south to north and from shelf to ocean. A similar distribution could be seen in the phosphate measurements which increased from south to north but two localised maxima (>0.4 μmol L^{-1}) could be seen in the data, one offshore and one onshelf which appeared to be linked to the outflow from The Minch, the narrow channel separating the Hebridean Islands from mainland Scotland. Silicate concentrations exceeded 2 μmol L^{-1} at inshore stations close to land but more generally were ~1.5 μmol L^{-1} on the shelf and decreased westwards towards the ocean. Variability in DIC concentrations was comparatively muted but higher concentrations were seen across much of the inner shelf. Alkalinity concentrations

were ~2325 μmol kg^{-1} on shelf, with the exception of those stations around the Isle of Lewis where concentrations were notably lower (<2315 μmol kg^{-1}).

The particulate pool concentrations were patchily distributed with the exception of POP and PIC, which exhibited moderate to strong lateral gradients between the innermost stations and outer shelf and offshore stations. Both POP and PIC concentrations were highest around the Isle of Lewis and rapidly reduced towards the open ocean. POC, PON and bSi concentrations show a varied distribution with a localised southern maxima along transect F at ~56°N (**Figure 2**). There was also a suggestion of elevated POC and PON concentrations around the Isle of Lewis to the north, but weaker indications of a comparable peak in bSi concentrations.

Cross-Shelf Sections

Several of the surface patterns described above extended to the seabed indicating well mixed shelf waters (**Figure 3**). Benthic water temperatures varied along and between transects, with the warmest waters (>13°C) found along the southernmost transect G. More generally, water temperatures were >11°C on the shelf, dropping below this at the shelf edge and across the upper continental slope as the depth increased. There was no indication of upwelling at the shelf break (determined by the position of the 9 °C isotherm) and examination of the wind direction timeseries for October and November revealed no sustained periods of northerly winds, which are known to induce upwelling in this region (Dickson *et al.,* 1986; 1988).

Absolute salinities were broadly similar along transects C to G revealing moderate cross-shelf gradients between the lower salinity waters of the inner shelf and the open

ocean. Along transect A a strong salinity gradient was observed due to the influence of the inshore Scottish Coastal Current, which reduced absolute salinities to ~34.9 g kg^{-1} at the inner most stations.

The resulting density sections revealed well-mixed waters with variable stratification though there was a clear difference in the proportion of shelf-like (warmer and fresher) and ocean-like (cooler and more saline) stations along each transect with transects A, C and G revealing more shelf-like conditions at their eastern extremities compared to the other transects.

Dissolved oxygen concentrations did not mirror the pattern seen in surface waters and a pronounced reduction in oxygen concentrations was observed with depth and along each transect at the seabed (**Figure 3**). At their lowest, oxygen concentrations were <250 μmol kg^{-1}, a reduction of ~30 μmol kg^{-1} with respect to typical surface concentrations and indicative of moderate microbial activity. The spatial extent and volume of the low oxygen region varied along each transect, being broadest along transect D and narrowest on transect G. Inshore stations were generally comparatively well oxygenated at depth, most likely due to shallow water column depths and deep mixing. The bolus of water with reduced oxygen concentrations was typically located between 100-400 m depth thus linked the outer shelf and upper continental slope.

As a result of both primary production in surface waters removing DIC, and respiratory processes in the deeper waters of the shelf and upper slope releasing DIC, a strong vertical gradient in DIC concentrations between surface waters and deeper waters on the shelf was evident (**Figure 4**). DIC concentrations reached local

maximum concentrations at the seabed and within the oxygen minimum regions with concentrations increasing from 2100-2120 μmol kg^{-1} in the upper 100 m to >2145 μmol kg^{-1} below 100 m, a typical increase of at least 25-40 μmol kg^{-1}. Maximum near bed DIC concentrations were ~2170 μmol kg^{-1}, but more commonly were in the range 2145-2165 μmol kg^{-1}. Relative to waters at the same depth offshore the near bed DIC concentrations were around 20 μmol kg^{-1} higher.

The distribution of particulate pools was equally patchy with depth as it was in surface waters. With the exception of transect F which revealed elevated POC, PON and POP concentrations at the shelf break, particulate concentrations reduced with depth and from inshore to offshore. It is possible that sediment resuspension at the shelf break explains the elevated concentration seen on transect F. Concentrations of POC were broadly comparable between transects with typical concentrations of 5-7.5 μmol L^{-1} present at depth over the shelf. Vertical gradients in PON concentration were more obvious between surface waters and those at depth but near seabed concentrations were generally >0.4 μmol L^{-1}. POP concentrations were <0.04 μmol L^{-1} and there was a tendency for elevated concentrations close to the shelf break on several transects. Perhaps because of lower concentrations, POP distributions were also less variable than either POC or PON concentrations. The concentration of bSi was generally 0.2-0.4 μmol L^{-1} close to the seabed, but was elevated on transect D. There was a suggestion of elevated bSi concentrations at depth offshore compared to inshore stations.

Circulation across the Shelf and Slope Current

VM-ADCP data clearly captured the Slope Current and the contrast between shelf and open ocean waters despite the patchy data coverage (**Figure 5**). The core of the Slope Current was captured along transects D, E, and F but it is less clear if the current was observed along transect G where the current was either comparatively weak and located at ~9.3°W or located beyond the western end of our transect. In the following we have assumed that the current was at 9.3°W. On transect C there is also a question mark over the position of the current given the limited data available for this transect. It is possible that the current was located between 9-9.5°W or >10°W given its position on other transects. If the latter possibility was true then we may just have resolved the eastern edge of the current at ~10°W, but given the apparent strengthening of the Slope Current towards the north it seems more likely that the Slope Current was not resolved on transect C. Along transect A the slope current was located above the 500 m bathymetric contour but we also observed a strong inshore current related to outflow from The Minch. Maximum depth averaged meridional current velocities ranged from 0.19 to 0.36 m s^{-1} (**Table 1**). To the west of the Slope Current on transects E and F there is evidence to suggest a southerly flow, whilst on the shelf to the east of the Slope Current northerly velocities were weaker and typically <0.2 m s^{-1}.

Air-Sea CO_2 Flux

Except for inshore stations immediately around the Isle of Lewis, the Hebrides Shelf was undersaturated in CO_2 with respect to the atmosphere with most pCO_2 values below 380 μatm. Air-sea CO_2 fluxes ranged from -14.6 to 12.4 mmol C m^{-2} d^{-1} (**Figure 6**). Six stations indicated positive air-sea CO_2 fluxes (i.e. outgassing to the atmosphere). All six stations were closely grouped, clustered around the Isle of Lewis,

and in shallow water. These six stations represented a sub-regional cluster indicative of important differences in CO_2 dynamics due to a localised mixing/circulation regime. Of these 6 stations, stations A1 and A2 were notable for low salinites (<35 g kg^{-1}) and low alkalinities, characteristic features indicating that these two stations were located in the outflow of the Scottish Coastal Current that flows northwards through The Minch. The other 4 stations with positive air-sea CO_2 fluxes (B1, C1, C2, & D1) generally had lower absolute salinities (~<35.3 g kg^{-1}) compared to stations further offshore (>35.4 g kg^{-1}) suggesting that they too were predominately influenced by inshore waters, possibly by terrestrial inputs and by part of the bifurcated Scottish Coastal Current that flows west of the Hebrides (McKay *et al.,* 1986; Inall *et al.,* 2009). More importantly however these stations were in shallow water and the water column was fully mixed. Collectively, the dataset revealed important regional gradients in the flux of CO_2 and in general inshore stations were weak CO_2 sinks (or CO_2 sources) whereas outer shelf and open ocean stations were stronger sinks.

Averaged in total or by region, the overall conclusion was that the region was a weak to moderate CO_2 sink. The cruise mean CO_2 sink (using all data) was -3.98 mmol C m^{-2} d^{-1}, whereas the Hebrides region (i.e. all stations inside the boundary shown in **Figure 1**) was a slightly weaker sink at -3.2 mmol C m^{-2} d^{-1}. The 7 stations west of the outer boundary, and therefore reflective of the open ocean were stronger CO_2 sinks with an average flux of -6.7 mmol C m^{-2} d^{-1}. Thus to first order the open ocean was approximately 2-fold stronger as a CO_2 sink than the shelf at this time and consequently a shelf to ocean gradient in the CO_2 sink can be inferred. The sub-regional cluster of stations around the Isle of Lewis with positive air-sea fluxes had an average outgassing flux of 5.3 mmol C m^{-2} d^{-1}.

To obtain a regional air-sea CO_2 flux we used the mean Hebrides flux (-3.2 mmol C m^{-2} d^{-1}) and an estimate for the spatial extent of the shelf covered by the survey (54,747 km^2) to produce a regional CO_2 sink estimate of -0.0021±0.0044 Tg C d^{-1}. The large standard deviation associated with this mean regional flux was due to the inclusion of those stations with a positive air-sea CO_2 flux around the Isle of Lewis. Exclusion of those stations resulted in a mean daily flux of -5.8 mmol C m^{-2} d^{-1} and a regional flux of -0.0038±0.0030 Tg C d^{-1}, suggesting that the outer shelf was most likely a stronger sink than inferred initially.

Shelf Edge Exchange

Estimates of transport based on maximum depth averaged currents along each transect are presented in **Table 1**. Offshore transports associated with the Ekman drain ranged from 0.74 to 2.68 m^2 s^{-1}, with a mean value of 1.81±0.79 m^2 s^{-1}. The corresponding downslope volume transports ranged from 0.38 to 1.38 Sv with a mean of 0.93±0.41 Sv. As both the transport and volume transport estimates are sensitive to the magnitude of the depth-averaged current our estimates should be considered as upper limits as we used maximum depth averaged current speeds in the above calculations due to the poor resolution of the current along some transects preventing calculation of a true mean current velocity. Similarly, we have not accounted for any variation in current strength with depth, which may also lead to an overestimation of current speeds and hence transports.

Also shown in **Table 1** are estimates for the wind-driven surface (onshore) flux. Ekman transports ranged from 1.89 – 2.2 m^2 s^{-1} with an average transport of

2.00±0.12 m^2 s^{-1}. The corresponding volume transports when scaled to the extent of the Hebrides Shelf edge (516 km) ranged from 0.98 to 1.13 Sv, with a mean of 1.05±0.06 Sv. The mean onshore surface flux of 1.05 Sv was therefore 13% larger than the mean offshore flux via the Ekman drain (0.93 Sv). Note however that on transects D and E the off-shelf flux via the Ekman drain exceeded the surface wind-driven on-shore flux, thus the larger overall mean surface flux does not adequately portray dominance of this flux term along all sectors of the Hebrides Shelf. As we cannot fairly extrapolate our results to an annual timescale this also means that the temporally localised dominance of the onshore flux over the offshore flux does not contradict more comprehensive analyses showing a mean downwelling flux in this region (Holt *et al.,* 2009).

To estimate particulate export fluxes the particulate pool concentrations (**Figure 4**) were first converted to their respective molar masses. PON, POP and bSi-opal fluxes varied significantly between transects, with 9-fold variability in PON, 8-fold variability in POP and 4-fold variability in bSi-opal fluxes. Mean particulate fluxes of 1.32±0.8 kg N m^{-1} d^{-1}, 0.12±0.07 kg P m^{-1} d^{-1}, and 2.9±1.26 kg opal m^{-1} d^{-1} were derived from the individual transect results (**Table 2**).

The concentration of POC near the seabed at shelf break stations ranged 4-fold from 42-209 mg m^{-3} with a mean concentration of 89 mg m^{-3}. Between each transect POC fluxes could vary significantly due to differences in both the transport term and the POC concentration measured at the shelf break. Consequently, our estimates of cross-shelf POC flux ranged from 2.7 kg C m^{-1} d^{-1} (based on transect G) to 28.4 kg C m^{-1} d^{-1} (based on transect F) highlighting the importance of small-scale heterogeneity in the

cross-shelf export of material latitudinally along the shelf edge (**Table 3**). The product of the mean Ekman drain transport (1.81 m^2 s^{-1}) and the mean POC concentration (89±63 mg m^{-3}) was an export flux of POC from the shelf to the continental slope and open ocean of 13.9 kg C m^{-1} d^{-1}, slightly larger than the true mean from the individual transects of 12.8 kg C m^{-1} d^{-1} (**Table 3**) due to spatial variability, or if scaled to the extent of the Hebrides shelf edge, a total off-shelf POC flux of 0.007±0.005 Tg C d^{-1}.

Deep-water PIC measurements were limited and the few available observations indicate PIC concentrations of between 1.3 and 7.2 mg C m^{-3} near the seabed (note that here we refer to weights of PIC as carbon not calcite). The mean concentration was 4.1±2.6 mg C m^{-3} (n = 4) for samples collected over a depth range of 107 – 193 m. Based on this mean value and using the mean bottom Ekman transport term (Table 1) we estimate a mean export of 0.64 kg C m^{-1} d^{-1}. However, 2 of the 4 samples were collected at ~190 m depth (1.3 – 5.2 mg C m^{-3}) providing a lower mean value of 3.2±2.8 mg C m^{-3} that may be more appropriate for evaluating the shelf export flux and which resulted in a lower export flux of 0.5 kg C m^{-1} d^{-1}. Both approximations are similar to the true mean of 0.6 kg C m^{-1} d^{-1} (**Table 3**), but fail to adequately portray the variability in the flux between transects. The export of carbon as PIC from the shelf via the Ekman drain was therefore an order of magnitude smaller than the export of carbon as POC. This may in part reflect the offshore position of most coccolithophore blooms in this region (Holligan 1986), which may limit sinking and deposition of PIC on the shelf.

Following similar arguments to the above it is possible to estimate the offshelf transport of DIC. We assessed this in two ways, firstly by using the total DIC

concentration and secondly by defining an excess concentration relative to offshore waters to reflect the accumulation of DIC in the deeper waters of the shelf. Total offshore fluxes of DIC ranged from 1.61 to 5.85 tonnes C m^{-1} d^{-1} by transect and averaged 3.94±1.72 tonnes C m^{-1} d^{-1} (**Table 3**). In contrast, and by using a typical excess of 20 μmol kg^{-1} as indicative of the difference between near bed DIC concentrations on shelf (source region) relative to open ocean waters at the same depth (receiving region), rather than the surface to seabed difference, we estimate that the Ekman drain could transport an excess of 0.037±0.016 tonnes C m^{-1} d^{-1} from the Hebrides Shelf to the open ocean. By transect the excess DIC flux ranged from 0.015 to 0.054 tonnes C m^{-1} d^{-1} (**Table 3**)

We also estimated the onshore fluxes in the surface Ekman layer using mean mixed layer concentrations calculated from offshelf stations on each transect. Onshore bSi-opal fluxes ranged from 2.2 to 5.0 (mean 3.5±1.0) kg opal m^{-1} d^{-1}, PON fluxes ranged from 1.3 to 2.1 (mean 1.7±0.3) kg N m^{-1} d^{-1}, and POP fluxes ranged from 0.16 to 0.28 (mean 0.23±0.04) kg P m^{-1} d^{-1} (**Table 2**). Similarly, total onshore DIC fluxes ranged from 4.05 to 4.69 tonnes C m^{-1} d^{-1}, and averaged 4.35±0.26 tonnes C m^{-1} d^{-1}. POC fluxes ranged from 12.1 to 17.1 kg C m^{-1} d^{-1}, and averaged 13.4±2.1 kg C m^{-1} d^{-1}. PIC fluxes were considerably smaller and ranged from 11.2 to 169.8 g C m^{-1} d^{-1} with an average of 80.8±69.7 g C m^{-1} d^{-1} (**Table 3**).

These results reinforce the importance of recognising spatial heterogeneity in the export or import of material along the shelf break. They also reveal that the total offshelf POC flux was approximately three times larger than the mean air-sea influx of CO_2, that the PIC flux was comparatively small compared to both POC and CO_2

fluxes and that all particulate carbon fluxes were small compared to the offshelf flux of DIC. However, dissolved organic carbon (DOC) represents the second largest reservoir of carbon in the ocean and before discussing a tentative carbon budget for this region we include in **Table 3** estimates of surface and deep DOC fluxes based on representative DOC concentrations obtained from the global synthesis of Barron and Duarte (2015) for comparison. Note that whilst our usage of the typical mean DOC concentrations for open ocean (63 μmol L^{-1}) and shelf waters (139 μmol L^{-1}) reported by Barron and Duarte (2015) results in the transect to transect variability being governed by the variability in the transport term alone, the apparent magnitude of these fluxes should be correct.

4. Discussion

4.1. CO_2 Fluxes

Air-sea CO_2 fluxes vary regionally and seasonally, and in temperate shelf sea systems are strongly influenced by biological productivity, local mixing regimes and prevailing wind speeds. Recent efforts to constrain global air-sea CO_2 fluxes in coastal seas highlight important seasonality and latitudinal variability (Chen *et al.,* 2013; Laruelle *et al.,* 2014). Our temporally limited observational dataset is therefore unlikely to provide a firm quantitative basis for calculating an annual flux for the Hebrides Shelf or more broadly for the NW European Shelf. Nevertheless, our mean daily air-sea CO_2 flux of -3.2 mmol C m^{-2} d^{-1}, is similar to a mean daily estimate of -3.5 mmol C m^{-2} d^{-1} derived from the mean annual estimate of -1.29 mol C m^{-2} yr^{-1}, reported for the NW European Shelf by Laruelle *et al.*, (2014). Our results may not therefore be significantly seasonally biased relative to the annual mean for the NW European Shelf and may also therefore be more broadly representative of the autumn

season (~September-December) rather than just the observation period (late October-Early November).

The annual CO_2 sink across the NW European Shelf has been estimated as -17.165 Tg C yr^{-1} (Laruelle *et al.,* 2014). By crudely extrapolating the regional daily air-sea CO_2 flux obtained in this study (-0.0021 Tg C d^{-1}) to a full year we estimate that the annual sink in this region would have been -0.77 Tg C yr^{-1}, or 4.5% of the entire NW European Shelf sink term estimated by Laruelle *et al*., (2014). As defined, the extended Hebrides Sea Region of 54,747 km^2 represents 4.9% of the area of the NW European Shelf (1112 $x10^3$ km^2), suggesting that the Hebrides Shelf was broadly representative of mean conditions across the NW European Shelf. However, this is based on the extrapolation of autumnal measurements across a full year and does not include the effects of seasonality and biological productivity, both of which are significant, so this calculation is only a qualitative indicator at best. It does however suggest that the Hebrides Shelf was broadly typical of the wider region and was neither an unseasonably strong sink nor source for CO_2 during autumn 2014. However, intra-regional variability in the sign of the air-sea CO_2 flux, and recognition that inner and outer shelf regions vary significantly in their ability to absorb/release CO_2 (e.g. Chen et al., 2013) can have a significant impact on the representative nature of our results.

4.2 Slope Current

The Hebrides Shelf region, and in particular the Slope Current, have been the focus of several previous studies. In **Table 4** we present literature observations of Slope Current velocities and/or volume transports measured using various methodologies. It

reveals significant variability between studies conducted at different latitudes, and between studies conducted in different years, supporting previous conjecture that there is substantial variability in the Slope Current in this region. Nevertheless, the majority of our observations (**Table 1**) lie within the range of previous observations.

The Extended Ellett Line (EEL) has sampled the shelf and slope areas at ~57°N at least annually since 1975 (Holliday and Cunningham 2013; Holliday *et al.,* 2015). The majority of EEL cruises were conducted in spring or summer with far fewer cruises conducted in autumn and almost none in winter. Nevertheless EEL cruises in 1996 (D223), 2005 (CD176) and 2006 (D312) were conducted in October and the VMADCP data from these cruises allows for a comparative study to the observations we report here. In **Table 5** we summarise our main findings. Despite crossing the shelf at similar latitudes (due to fixed station positions) there is considerable variability in the appearance of the Slope Current in the EEL cruise datasets. For example, the apparent width of the current varied almost 4-fold from 19 km at its narrowest (October 2006) to 76 km at its widest (October 2005). Whilst latitudinal variability in the Slope Current width was recognised by Dickson *et al*., (1986), there appears to be limited description in the literature of changes in Slope Current width on interannual timescales. Similarly, but to a smaller extent, the depth averaged current velocities varied over 2-fold between observation periods with the strongest observed current of 0.49 m s^{-1} occurring during the period of widest current (October 2006). The variability in both current width and depth averaged current velocities also impacts the apparent volume transport associated with the current, which ranged from 0.53 Sv to 1.48 Sv. Such transport estimates are in keeping with other independent estimates of the current transport, and our new observations, but the acoustic

penetration of the VMADCP also impacts the accuracy of these estimates. As there is considerable variability in the depth to which the current was resolved on each EEL cruise, varying from 275 m to 400 m, the apparent volume transports are susceptible to several errors (the same is true of our results). It is however, reassuring that approximately the same magnitude for the Slope Current volume transport can be obtained from different VMADCP datasets collected over an 18-year period (1996-2014). Nevertheless, the long-term mean geostrophic volume transport calculated by Holliday *et al*., (2015) from mean EEL hydrographic profiles across the Rockall Channel indicated a larger mean volume transport of 1.8±0.4 Sv associated with the Slope Current, which suggests that direct observation of the Slope Current by VMADCP underestimates the true transport (though note that the geostrophic estimate is itself biased by the seasonal distribution of EEL cruises). In light of the mean geostrophic transport estimate, comparable estimates of the volume transport from EEL cruises and from the literature, the unusually high transport estimate of 4 Sv calculated for transect F (**Table 1**) looks increasingly anomalous. At the western end of transect F (**Figure 5**) there was a strong southerly flow which in conjunction with equally strong northerly flows to the immediate east (~9.8°W) most likely signified the presence of a cyclonic eddy along the western edge of the current, thus biasing our volume transport estimates for this transect. Confirmation of this was found in satellite altimetry data, which revealed a sea level anomaly consistent with a cyclonic eddy, centred just north of the midway point between stations F5 and F6.

4.3. Surface Ekman Fluxes

Our surface wind-driven Ekman fluxes appear larger than typical flux estimates reported in the literature, which are often based on annually averaged data (e.g. 1.17

m^2 s^{-1}; Huthnance 2010). Significant seasonal variability in the surface Ekman flux term is recognised however and when viewed in this context our average transport of 2.04±0.12 m^2 s^{-1} (**Table 1**) is not too dissimilar to the mean winter value of 1.73 m^2 s^{-1} reported by Huthnance *et al.*, (2009) or the mean annual value of 1.71 m^2 s^{-1} derived from the results of Wakelin *et al.,* (2012). There is also the possibility that wind speeds and wind directions during Oct-Nov 2014 were favourable for onshore transport. The region experiences prevailing westerly winds and during the observation period strong southerly winds were dominant and these may have enhanced the onshore surface flux, particularly as the Hebrides Shelf is broadly orientated north-south.

4.4. Ekman Drain and Fluxes

Our estimates of the offshelf down-slope transport via the Ekman drain (**Table 1**) are similar to the few previous estimates available for this shelf (**Table 6**). This is largely due to the broad consistency of Slope Current velocities between studies (**Table 4**). For example, Simpson and McCandliss (2013) reported peak Slope Current velocities of 0.3 m s^{-1} at 56.47°N, and a mean Ekman drain transport of 1.6 m^2 s^{-1}, which if scaled to the Hebrides Shelf (516 km) would translate to a total volume transport of 0.83 Sv. Our new observations compare well to these measurements with a mean transport of 1.81 m^2 s^{-1} and mean volume transport of 0.93 Sv (**Table 6**). Aside from model based estimates, which represent the majority of previous attempts to quantify the Ekman drain, the only other direct observation we have identified by de Souza *et al*., (2001) indicated a lower transport of 0.46 m^2 s^{-1} and a volume transport of 0.3 Sv. This almost certainly results from use of a lower current velocity derived from summer observations compared to those measured here (**Table 4**). Despite these

differences results from these observational studies do compare favourably to modelled estimates of the offshelf transports suggesting that the region may be comparatively well represented in numerical models though there is a clear need for additional observations to better constrain these transports (**Table 6**).

Despite our offshelf down-slope transports exhibiting an almost 4-fold variation between transects the mean transport of 1.81 m^2 s^{-1} was comparable to the mean estimate of 1.75 m^2 s^{-1} obtained by Holt and Proctor (2008) based on a 40 year model run for the region. This suggests that conditions during October-November 2014 were near to (model) mean conditions (i.e. neither strongly enhanced or weakened). However, Xu *et al*., (2015) describe important seasonal to interdecadal variability in the Slope Current that will impact the variability in down-slope transport over similar timescales, which in addition to the 4-fold variability we highlight between transects, suggests that the flux of material offshelf is likely to be highly variable along the shelf break over a range of timescales.

Our estimates of downslope carbon flux are therefore harder to constrain. By scaling the mean offshelf flux of organic carbon (as POC; 12.75±9.48 kg C m^{-1} d^{-1}) associated with the Ekman drain to the length of the shelf break studied here (516 km) we obtain a total offshelf POC flux of 0.007±0.005 Tg C d^{-1} which matches the modelled total organic carbon flux of 0.007 Tg C d^{-1} obtained by Wakelin *et al.,* (2012) for a slightly larger sector of the NW European shelf (~52-60°N; ~1000 km shelf break length). Clearly, extrapolation of our per unit length cross shelf flux to the same shelf break length used in the Wakelin study would effectively double the resulting offshelf POC flux associated with the Ekman drain and greatly exceed the

model estimate of total organic carbon flux. Whilst this suggests that differences in organic carbon flux between the observations and the model may be significant we caution against over interpretation of this result as our own observations show the cross shelf flux to be highly spatially heterogeneous and unlikely to persist at our mean flux rate over large spatial distances or at a fixed value throughout the year. This further suggests that global extrapolations from limited observations may contain significant errors. Nevertheless, both flux estimates are 14-fold larger than the estimate of 0.0005 Tg C d^{-1} obtained by scaling the single observation of 0.99 kg C m^{-1} d^{-1} reported by Simpson and McCandliss (2013) at ~56.5°N to the extent of the Hebrides shelf edge, suggesting that cross shelf fluxes of organic carbon remain poorly quantified both observationally and in models. Differences between Simpson and McCandliss (2013) and the present study may be explained given the transport variability between transects reported here, suspected seasonality in such transport terms, and differences in methodologies used for determining POC concentrations (transmissometer/suspended particulate matter relationship vs elemental analysis). Despite such uncertainties our results suggest that downslope POC fluxes are significant compared to air-sea CO_2 fluxes, for example. Our results also imply that the downslope POC flux is probably highly significant for the benthic communities of the continental slope that rely upon a supply of organic carbon from surface waters. At present, and with the data available, it is unclear how this flux and its importance for benthic communities, would vary seasonally, nor over what distance this material would be deposited. Simple calculations assuming an even deposition of the exported POC over the seabed between 200 and 2000 m depth (~50 km distance) suggest an average flux of 0.24±0.18 g C m^{-2} d^{-1} (88±65g C m^{-2} yr^{-1}), somewhat larger than typical benthic respiration rates 0.05 g C m^{-2} d^{-1} (20 g C m^{-2} yr^{-1}) assumed for this

region (Simpson and McCandliss 2013). It is probable that the majority of this material is remineralized within the water column.

Although the offshelf flux of POC represents only ~0.3% of the total offshelf carbon flux, which is dominated by DOC (6.1%) and DIC (93.6%), it is instructive to consider the global significance of the downslope POC flux from the Hebrides Shelf. To do so we compared our results to similar findings from the East China Sea and to a mass balance derived global shelf sea carbon budget. Chen and Wang (1999) reported an offshelf downslope POC flux from the East China Sea of 695 $x10^9$ mols C yr^{-1}. This equates to a daily flux of 0.02 Tg C d^{-1}, approximately 3-fold larger than we report for the Hebrides Shelf (0.007 Tg C d-1) despite the East China Sea being ~16-fold larger in area. If we convert both downslope estimates to a per unit area basis using the respective shelf areas we find a mean downslope POC export of 2.1 mmols C m^{-2} d^{-1} for the East China Sea and 10.01 mmols C m^{-2} d^{-1} for the Hebrides Shelf (**Table 7**). This suggests a stronger export potential for the Hebrides Shelf compared to the East China Sea.

Based on a global synthesis of shelf sea carbon fluxes and a mass balance calculation Chen et al (2003) estimated a global downslope POC flux of 20 x 10^{12} mol C yr^{-1}. Converting this to a daily per unit area flux using a global shelf area of 26 x 10^6 km we obtain a daily flux of 2.11 mmol C m^{-2} d^{-1}. Thus our estimate of the offshelf downslope POC flux of 10.01 mmol C m^{-2} d^{-1} for the Hebrides Shelf is ~5 fold larger than the global mean. However, we urge caution in the interpretation of these comparisons as the offshelf flux of POC from the Hebrides Shelf may integrate over a larger shelf area than we have defined and an increase in shelf surface area would

decrease the per unit area flux (i.e. the offshelf flux could include POC from inshore waters or the Irish Sea). Nevertheless, the Hebrides Shelf appears to be a prominent source of POC with a total offshelf flux (0.007 Tg C d^{-1}/ 12.75 kg C m^{-1} d^{-1}) that represents ~1% of total global downslope POC export from shelf seas (0.66 Tg C d^{-1}; based on Chen *et al*., 2003) despite representing only 0.21% of global shelf sea area. An alternative calculation based on a global shelf break length of 150,000 km (Jahnke 2010) implies a global mean POC export of 4.38 kg C m^{-1} d^{-1}, which implies that the Hebrides Shelf exported 2.9-fold more carbon per metre of shelf break than the global mean, whilst representing 0.34% of global shelf break length. Thus regardless of either shelf area or shelf break length the Hebrides Shelf is exporting more particulate carbon per unit of measure than the global mean.

The inorganic carbon flux, which dominates the flux of total carbon, was estimated in two ways (**Table 3**). Under the first approach our total inorganic carbon flux (PIC + DIC excess (DICxs); 36.62 kg C m^{-1} d^{-1} equivalent to 0.019 Tg C d^{-1}) was considerably smaller than the modelled flux of 2.548 Tg C d^{-1} reported by Wakelin *et al*., (2012). This was due to our use of the DIC excess in near bottom waters relative to waters at the same depth offshore rather than the absolute DIC concentration to assess the offshelf flux. Repeating this comparison for total DIC content using representative DIC concentrations of 2145 to 2169 μmol kg^{-1} by transect (**Figure 4**) we obtained a total inorganic carbon flux (DIC + PIC) of 3.94±1.72 tonnes C m^{-1} d^{-1} (2.034±0.89 Tg C d^{-1}) (**Table 3**), which was only ~20% smaller than the model flux implying that modelled fluxes of inorganic carbon may be better understood than fluxes of organic carbon.

Based on the calculation of excess DIC, which provides an indication of the net exportable pool of DIC in the benthic layer of the shelf (36.62±16.0 kg C m^{-1} d^{-1}; 0.019 Tg C d^{-1}), we estimate that the mean air-sea CO_2 flux for the region would have represented 11% of the excess DIC pool compared to only ~1% of the total DIC pool flux.

In **Figure 7** we present a provisional carbon budget for the outer Hebrides Shelf region based on total carbon fluxes in both surface and bottom Ekman layers. We have augmented this with estimated fluxes of dissolved organic carbon (DOC) based on the representative DOC concentrations reported by Barron and Duarte (2015) of 63 μmol L^{-1} and 139 μmol L^{-1} for open ocean and shelf waters respectively (**Table 3**). This budget reveals that i) the mean onshore total carbon flux was 6% larger than the mean offshore total carbon flux (though the net flux on an individual transect could be onshore or offshore with a net difference of up to ~60%; **Table 3**), ii) there was a net onshore flux of DIC, driven by the larger surface Ekman flux, despite increased DIC concentrations at depth (though again note the transect to transect variation; **Table 3**), iii) there was a net offshore flux of PIC possibly due to resuspended material near the seabed, iv) assuming that the DOC concentrations are appropriate for the region and time of year, a net offshore flux of DOC, which supports the global analysis of Barron and Duarte (2015), and v) the net flux of POC was approximately 0 (due to rounding) but a small import of POC of ~0.5 kg C m^{-1} d^{-1} may have been more likely (**Table 3**).. We include our regional mean air-sea CO_2 flux, noting that it is highly probable that inshore waters would have contributed to an outgassing of CO_2 at this time given the spatial patterns in our own data (Figure 6) and recent syntheses showing marked differences between inner shelf and outer shelf regions (Chen *et al.*, 2013). To

facilitate comparison of our results with other shelf systems we have also converted the individual offshelf transect particulate fluxes to a per unit area basis based on the shelf area studied (i.e. 54,747 km^2; **Table 7**). Note that such conversions are sensitive to the choice of area used. Nevertheless, mean particulate fluxes of 10.01 mmol C m^{-1} d^{-1}, 0.89 mmol N m^{-2} d^{-1}, and 0.04 mmol P m^{-2} d^{-1} for POC, PON and POP respectively and 0.47 mmol C m^{-2} d^{-1} and 0.41 mmol opal m^{-2} d^{-1} for PIC and bSi-opal fluxes resulted. Based on these mean fluxes the mean stoichiometric C:Si:N:P content of the exported particulate material was 250:10:22:1.

Based on the total carbon flux of 2.32 Tg C d^{-1} (4.50±0.26 tonnes C m^{-1} d^{-1}) the onshore flux of organic carbon (DOC and POC) represented ~3.3% of the total onshore carbon flux whilst inorganic carbon (DIC and PIC) represented ~96.7%. This compares well to the estimated inorganic carbon content of inflowing waters of 97% reported for the North Sea by Thomas *et al.,* (2005). However, within the offshore flux associated with the Ekman drain 2.18 Tg C d^{-1} (4.21±1.84 tonnes C m^{-1} d^{-1}) organic carbon represented 6.4% on average with inorganic carbon representing 93.6%. Thus, despite the net flux of carbon being onshore, the offshelf flux of carbon contained a significantly larger organic component than the onshore flux. Within this organic component an average of 95% was represented by dissolved organic carbon and 5% by particulate organic carbon thus demonstrating the significance of dissolved fractions for organic carbon export from coastal seas. Viewed against these larger total carbon fluxes the mean air-sea flux of CO_2 was comparable to 30% of the offshelf POC flux, ~1.4% of the total offshelf organic carbon flux, and <0.1% of the total offshelf carbon flux.

How is the offshelf organic carbon flux sustained? It is unlikely that our measured POC flux persists at its measured magnitude year round and indeed models of the NW European Shelf show strong seasonality in carbon fluxes and primary production (Wakelin *et al.,* 2012; Artioli *et al.,* 2014). It is highly probable therefore that the accumulation of organic matter beneath the mixed layer has a seasonal component to it and that the offshelf fluxes of biogenic material we have calculated are towards upper potential values. We base this assessment on the knowledge that the development of an exportable reservoir of organic material will be linked to the residence time of the shelf, which can be measured in months due to weak residual flows and on established seasonality in the Slope Current which ultimately drives any cross shelf transport. Globally the mean coastal ocean residence time is ~130 days (Huthnance 1995). In the Hebrides Shelf region monitoring of ^{137}Cs discharges from the Sellafield nuclear reprocessing plant indicate that residence times may be longer, possibly over 1 year (Prandle 1984), and even within identifiable currents such as the Scottish Coastal Current it is estimated to take ~9 months for ^{137}Cs to transit from the Irish Sea to the mid Hebrides Shelf region (McKay *et al.,* 1986; McCubbin *et al.,* 2002). Long residence times will therefore allow for the retention and accumulation of material from the productive spring and summer months which, if not remineralised upon settling beneath the mixed layer and instead retained within an unconsolidated benthic fluff layer (Jago *et al.,* 1993), may ultimately become entrained into the Ekman drain and exported offshore. Neither the lability or age of the DOC fraction is known and the long-term consequences of a net flux of organic carbon from the shelf to the ocean requires further investigation, a topic previously highlighted by Barron and Duarte (2015). Long residence times, coupled with weak cross-shelf exchange, may also explain two other interesting attributes of our

observational dataset, specifically the (seasonal) accumulation of excess DIC and the lower oxygen waters seen beneath the mixed layer over extensive sections of the shelf; features which although common for the NW European Shelf nevertheless require time and quiescent conditions to form within.

4.5 Limitations and Wider Applications

This study presents a detailed observational assessment of the Ekman drain for the Hebrides Shelf and indicates that there is a significant export of organic carbon to the open ocean, as well as significant variability in export fluxes along the shelf break. Nevertheless, the dataset we present here is not perfect. Obvious weaknesses include the patchy VMADCP coverage, the horizontal sampling resolution, which was relatively crude compared to the width of the Slope Current, and the westward extent of sampling, which may not have fully resolved the true western boundary of the Slope Current on all transects. Nevertheless, our measurements of the Slope Current itself are comparable with previous observations and with recent modelled fluxes, and our carbon fluxes agree well with prior measurements and shelf-wide synthesis efforts, suggesting that the limitations of the data may not significantly impact the overall conclusions.

It is not appropriate however to extrapolate our observations more widely along the edge of the NW European shelf as both models and observations show that currents and transports tend to be weaker further south and significantly stronger further north. Consequently we would overestimate fluxes in the south or underestimate them further north using the mean results obtained along the Hebrides Shelf. In addition, the 4-fold variability we report in the bottom Ekman transport and up to 9-fold

variability in particulate concentrations argues for caution in regional or global extrapolations from limited data. However, poleward flowing slope currents are a common feature globally (Hill *et al.*, 1998) thus the potential magnitude of offshelf carbon fluxes associated with the Ekman drain may be significant at a global level. Widely recognised limitations in data coverage though have to date prevented detailed quantification of the cross shelf exchange of carbon at the global scale (Liu *et al.*, 2010 and references therein). Nevertheless, a simple calculation using our mean Ekman drain transport estimate and carbon pool concentrations and a global shelf break length of 1.5 $x10^5$ km (Jahnke 2010) provides an order of magnitude estimate of total carbon flux of ~0.6 Pg C d^{-1} or ~230 Pg C yr^{-1}, the vast majority of which is DIC. This estimate however is 6.5 times larger than a global estimate of DIC transport reported by Chen *et al* (2003) and neatly demonstrates how much we still have to learn about the coastal ocean.

5. Conclusions

During October and November 2014 the Hebrides Shelf was a moderate sink for atmospheric CO_2, with a mean shelf wide air-sea CO_2 flux of -3.2 mmol C m^{-2} d^{-1}. This equated to a total regional sink of -0.0021 Tg C d^{-1}, comparable to estimates derived from more extensive database analyses. Transport of carbon off shelf via the downwelling circulation that is typical of this shelf region, resulted in a total offshelf carbon flux of 2.18 Tg C d^{-1} (4.21 tonnes C m^{-1} d^{-1}), of which 93.6% was inorganic and 6.4% was organic with DOC representing 95% of the organic flux. On a per unit area basis the export of POC from the Hebrides Shelf of 10.01 mmol C m^{-2} d^{-1} was found to be 5 times larger than the global mean. An equivalent calculation based on global shelf break length indicated the mean offshelf POC flux of 12.75 kg C m^{-1} d^{-1}

was ~3-fold larger than the global mean. Consequently the total offshelf POC flux of 0.007 Tg C d^{-1} could represent ~1% of total global downslope POC export making the Hebrides Shelf a potentially significant source of POC to the continental slope and neighbouring northeast Atlantic Ocean. We estimate this mechanism could supply the ocean benthos with a daily average particulate carbon flux of 0.24±0.18 g C m^{-2} d^{-1}.

Acknowledgments

We thank the following for access to data, ECMWF for the ERA-Interim product (http://apps.ecmwf.int/datasets/), and the NOAA-ESRL Physical Sciences Division, Boulder Colorado for NCEP-II reanalysis products (http://www.esrl.noaa.gov/psd/) and global CO_2 records (http://www.esrl.noaa.gov/gmd/ccgg/trends/global.html#global). We also thank the anonymous reviewer, editor and John Huthnance for comments on an earlier version of this paper. L.A. Salt held post-doctoral grants from the Conseil Général du Finister and Région Bretagne. Cruise DY017 was a NERC National Capability funded cruise conducted in support of the UK NERC/DEFRA co-funded Shelf Sea Biogeochemistry programme (NE/K001701/1). Data are available via the British Oceanographic Data Centre (www.bodc.ac.uk) or from the authors.

References

Artioli, Y., J.C. Blackford, G. Nondal, R.G.J. Bellerby, S.L. Wakelin, J.T. Holt, M. Butenschön and J.I. Allen (2014). Heterogeneity of impacts of high CO2 on the North Western European Shelf. Biogeosciences 11, 601-612.

Barron, C. and C.M. Duarte (2015). Dissolved organic carbon pool and export from the coastal ocean. Global Biogeochemical Cycles 29, doi: 10.1002/2014GB005056.

Bauer, J.E., W-J. Cai, P.A. Raymond, T.S. Bianchi, C.S. Hopkinson and P.A.G. Regnier (2013). The changing carbon cycle of the coastal ocean. Nature 504, 61-70.

Baxter, J.M., I.L. Boyd, M. Cox, A.E. Donald, S.J. Malcolm, H. Miles, B. Miller and C.F. Moffat (2011). Scotland's Marine Atlas: Information for the national marine plan. Edinburgh, Marine Scotland**:** 191 pp.

Booth, D.A. and D.J. Ellett (1983). The Scottish continental slope current. Continental Shelf Research 2(2/3), 127-146.

Borges, A.V. (2005). Do we have enough pieces of the jigsaw to integrate CO_2 fluxes in the coastal ocean? Estuaries 28(1), 3-27.

Carter, D.J.T., J. Loynes and P.G. Challenor (1987). Estimates of extreme current speeds over the continental slope off Scotland. Wormley, UK, Institute of Oceanographic Sciences, Report No. **239:** 143 pp.

Chafik, L., T. Rossby and C. Shrum (2014). On the spatial structure and temporal variability of poleward transport between Scotland and Greenland. Journal of Geophysical Research: Oceans 119, 824-841, doi: 810.1002/2013JC009287.

Chen, C.-T.A., and S.-L. Wang (1999). Carbon, alkalinity and nutrient budgets on the East China Sea continental shelf. Journal of Geophysical Research 104(C9), 20,675-620,686.

Chen, C.-T.A., K.-K. Liu and R. Macdonald (2003). Continental margin exchange. *in* Ocean Biogeochemistry. M. J. R. Fasham (Editor). Berlin, Springer**:** 53-97.

Chen, C.-T.A., T.-H. Huang, Y.-C. Chen, Y. Bai, X. He and Y. Kang (2013). Air-sea exchanges of CO_2 in the world's coastal seas. Biogeosciences 10, 6509-6544.

Dickson, A.G., C.L. Sabine and J.R. Christian (2007). Guide to best practices for ocean CO_2 measurements. PICES Special Publication 3**:** 191 pp.

Dickson, R.R., P.M. Kelly, J.M. Colebrook, W.S. Wooster and D.H. Cushing (1988). North winds and production in the eastern North Atlantic. Journal of Plankton Research 10(1), 151-169.

Dickson, R.R., W.J. Gould, C. Griffiths, K.J. Medler and E.M. Gmitrowicz (1986). Seasonality in currents in the Rockall Channel. Proceedings of the Royal Society of Edinburgh 88B, 103-125.

Egbert, G.D., A. Bennett and M. Foreman (1994). TOPEX/Poseidon tides estimated using a global inverse model. Journal of Geophysical Research 99, 24,821-824,852.

Egbert, G.D., S. Y. Erofeeva and R. D. Ray (2010). Assimilation of altimetry data for nonlinear shallow-water tides: quarter-diurnal tides of the Northwest European Shelf. Continental Shelf Research 30, 668-679.

Egbert, G.D. and S.Y. Erofeeva (2002). Efficient inverse modelling of barotropic ocean tides. . Journal of Atmospheric and Oceanic Technology 19, 183-204.

Firing, E. and J.M. Hummon (2010). Shipboard ADCP measurements. he GO-Ship Repeat Hydrography Manual: A collection of expert reports and guidelines, ,

IOCCP Report No. 14, ICPO Publication Series No. 134. . **Version 1, 2010: 1-11.**

Green, D.R.H., M.J. Cooper, C.R. German and P.A. Wilson (2003). Optimization of an inductively coupled plasma - optical emission spectrometry method for the rapid determination of high-precision Mg/Ca and Sr/Ca in foraminiferal calcite. Geochemistry, Geophysics, Geosystems 4(6), 8404, doi:8410.1029/2002GC000488.

Hill, A.E., B.M. Hickey, F.A. Shillington, P.T. Strub, K.H. Brink, E.D. Barton and A.C. Thomas (1998). Eastern ocean boundaries *in* The Global Coastal Ocean: Regional Studies and Syntheses. A. R. Robinson and K. H. Brink. New York, John Wiley and Sons, Inc. The Sea: Vol. 11**:** 29-67.

Holliday, N.P. and S.A. Cunningham (2013). The Extended Ellett Line: Discoveries from 65 years of marine observations west of the UK. Oceanography 26(2), 126-163.

Holliday, N.P., S.A. Cunningham, C. Johnson, S.F. Gary, C. Griffiths, J.F. Read and T. Sherwin (2015). Multi-decadal variability of potential temperature, salinity and transport in the eastern sub-polar North Atlantic. Journal of Geophysical Research: Oceans 120, 5945-5967, doi:5910.1002/2015JC010762.

Holligan, P.M. (1986). Phytoplankton distributions along the shelf break. Proceedings of the Royal Society of Edinburgh 88B, 239-263.

Holt, J. and R. Proctor (2008). The seasonal circulation and volume transport on the northwest European continental shelf: A fine-resolution model study Journal of Geophysical Research 113, C06021, doi: 06010.01029/02006JC004034.

Holt, J., S. Wakelin and J. Huthnance (2009). Down-welling circulation of the northwest European continental shelf: A driving mechanism for the continental shelf carbon pump. Geophysical Research Letters 36, L14602, doi: 14610.11029/12009GL038997.

Huthnance, J.M. (1986). The Rockall slope current and shelf-edge processes. Proceedings of the Royal Society of Edinburgh 88B, 83-101.

Huthnance, J.M. (1995). Circulation, exchange and water masses at the ocean margin: the role of physical processes at the shelf edge. Progress in Oceanography 35, 353-431.

Huthnance, J.M. (2010). The northeast Atlantic margins. *in* Carbon and Nutrient Fluxes in Continental Margins. K.-K. Liu, L. Atkinson, R. Quiñones and L. T.-M. (Eds). Berlin Heidelberg, Springer-Verlag**:** 215-234.

Huthnance, J.M., J.T. Holt and S.L. Wakelin (2009). Deep ocean exchange with west-European shelf seas. Ocean Science 5, 621-634.

Huthnance, J.M. and W.J.Gould (1989). On the northeast Atlantic Slope Current. *in* Poleward Flows along Eastern Ocean Boundaries S.J. Neshyba, C.N.K. Mooers, R.L. Smith and R.T. Barber (Eds.). Coastal and Estuarine Studies 34**:** 374 pp.

Hydes, D.J., M. Aoyama, A. Aminot, K. Bakker, S. Becker, S. Coverly, A. Daniel, A. G. Dickson, O. Grosso, R. Kerouel, J. van Ooijen, K. Sato, T. Tanhua, E. M. S. Woodward and J. Z. Zhang (2010). Determination of dissolved nutrients (N, P, Si) in seawater with high precision and inter-comparability using gas-segmented continuous flow analysers. The GO-Ship Repeat Hydrography Manual: A collection of expert reports and guidelines, IOCCP Report No. 14, ICPO Publication Series No. 134. **Version 1, 2010:** 1-87.

Inall, M., P. Gillibrand, C. Griffiths, N. MacDougal and K. Blackwell (2009). On the oceanographic variability of the North-West European Shelf to the west of Scotland. Journal of Marine Systems 77, 210-226.

IOC SCOR and IAPSO (2010). The International Thermodynamic Equation of Seawater - 2010: Calculation and use of thermodynamic properties, Intergovernmental Oceaonographic Commission. **Manuals and Guides No. 56 UNESCO,:** 196 pp.

Jago, C.F., A.J. Bale, M.O. Green, M.J. Howarth, S.E. Jones, I.N. McCave, G.E. Millward, A.W. Morris, A.A Rowden and J.J Williams (1993). Resuspension processes and seston dynamics. Philosophical Transactions of the Royal Society A 343, 475-491.

Jahnke, R.A. (2010). Global Synthesis. *in* Carbon and Nutrient Fluxes in Continental Margins. Global Change : The IGBP Series. K.-K. Liu, L. Atkinson, R. Quinones and L. Talaue-McManus (Eds.). Berlin, Springer-Verlag,**:** 597-615.

Jiang, L.-Q., W-J. Cai, R. Wanninkhof, Y. Wang and H. Luger (2008). Air-sea CO_2 fluxes on the U.S. South Atlantic bight: Spatial and seasonal variability. Journal of Geophysical Research 113, C07019, doi: 07010.01029/02007JC004366.

Kanamitsu, M., W. Ebisuzaki, J. Woollen, S-K Yang, J.J.. Hnilo, M. Fiorino and G.L. Potter (2002). NCEP-DOE AMIP-II Reanalysis (R-2). Bulletin of the American Meteorological Society, 1631-1643.

Kirkwood, D.S. (1996). Nutrients: Practical notes on their determination in seawater. ICES Techniques in Marine Environmental Sciences Report 17. Copenhagen, International Council for the Exploration of the Seas**:** 25pp.

Langdon, C. (2010). Determination of dissolved oxygen in seawater by Winkler titration using the amperometric technique. The GO-Ship Repeat Hydrography Manual: A collection of expert reports and guidelines, IOCCP Report No. 14, ICPO Publication Series No. 134. **Version 1, 2010:** 1-18.

Laruelle, G.G., R. Lauerwald, B. Pfeil and P. Regnier (2014). Regionalized global budget of the CO2 exchange at the air-water interface in continental shelf seas. Global Biogeochemical Cycles 28, 1199–1214, doi:1110.1002/2014GB004832.

Liu, K.-K., L. Atkinson, R. Quinones and L. Talaue-McManus (2010). Carbon and nutrient fluxes in continental margins. Berlin, Springer-Verlag, 741 pp

McCubbin, D., K.S. Leonard, J. Brown, P.J. Kershaw, R.A. Bonfeld and T. Peak (2002). Further studies of the distribution of technetium-99 and caesium-137 in UK and European coastal waters. Continental Shelf Research 22, 1417-1445.

McKay, W.A., J.M. Baxter, D.J. Ellett and D.T. Meldrum (1986). Radiocaesium and circulation patterns west of Scotland. Journal of Environmental Radioactivity 4, 205-232.

Orr, J.C., J.-M. Epitalon and J.-P. Gattuso (2015). Comparison of ten packages that compute ocean carbonate chemistry. Biogeosciences 12, 1483-1510.

Pelletier, G., E. Lewis and D. Wallace (2007). CO2SYS.XLS A calculator for the CO_2 system in seawater for Microsoft Excel/VBA. Washington State Department of Ecology/ Brookhaven National Laboratory, Olympia, WA/Upton, NY, USA.

Pingree, R.D. (1993). Flow of surface waters to the west of the British Isles and in the Bay of Biscay. Deep Sea Research Part II 40(1-2), 369-388.

Prandle, D. (1984). A modelling study of the mixing of ^{137}Cs in the seas of the European Continental Shelf. Philosophical Transactions of the Royal Society A 310, 407-436.

Proctor, R., F. Chen and P.B. Tett (2003). Carbon and nitrogen fluxes across the Hebridean shelf break, estimated by a 2D coupled physical-microbiological model. The Science of the Total Environment 314-316, 787-800.

Ragueneau, O. and P. Treguer (1994). Determination of biogenic silica in coastal waters: applicability and limits of the alkaline digestion method. Marine Chemistry 45, 43-51.

Raimbault, P., F. Diaz, W. Pouvesle and B. Boudjellal (1999). Simultaneous determination of particulate organic carbon, nitrogen and phosphorous collected on filters, using a semi-automatic wet-oxidation method. Marine Ecology Progress Series 180, 289-295.

Regnier, P., P.Friedlingstein, P. Ciais, F. T. Mackenzie, N. Gruber, I. A. Janssens, G. G. Laruelle, R. Lauerwald, S. Luyssaert, A. J. Andersson, S. Arndt, C. Arnosti, A. V. Borges, A. W. Dale, A. Gallego-Sala, Y. Goddéris, N. Goossens, J. Hartmann, C. Heinze, T. Ilyina, F. Joos, D. E. LaRowe, J. Leifeld, F. J. R. Meysman, G. Munhoven, P. A. Raymond, R. Spahni, P. Suntharalingam and M. Thullner (2013). Anthropogenic perturbation of the carbon fluxes from land to ocean. Nature Geoscience 6, 597-606.

Simpson, J.H. and R.R. McCandliss (2013). "The Ekman Drain": a conduit to the deep ocean for shelf material. Ocean Dynamics 63, 1063-1072.

Souza, A.J., J.H. Simpson, M. Harikrishnan and J. Malarkey (2001). Flow structure and seasonality in the Hebridean slope current. Oceanologica Acta 24(Supplementary), S63-S76.

Takahashi, T., S. C.Sutherland, R. Wanninkhoff, C. Sweeney, R. A. Feely, D. W. Chipman, B. Hales, G. Friederich, F. Chavez, C. Sabine, A. Watson, D. C.E .Bakker, U. Schuster, N. Metzl, H. Yoshikawa-Inoue, M. Ishii, T. Midorikawa, Y. Nojiri , A. Kortzinger, T. Steinhoffm, M. Hoppema, J. Olafsson, T. S. Arnarson, B. Tilbrook, T. Johannessen, A. Olsen, R. Bellerby, C.S.Wong, B. Delille, N.R.Bates and H.J.W. deBaar (2009). Climatological mean and decadal change in surface ocean pCO_2, and net sea–air CO_2 flux over the global oceans. Deep Sea Research Part II 56, 554-577.

Thomas, H.E., Y. Bozec, K. Elkalay and H.J.W. De Baar (2004). Enhanced open ocean storage of CO_2 from shelf sea pumping. Science 304, 1005-1008.

Thomas, H., Y. Bozec, H.J.W. de Baar, K. Elkalay, M. Frankignouelle, L.-S. Schiettecatte, G. Kattner and A.V. Borges (2005). The carbon budget of the North Sea. Biogeosciences 2, 87-96.

Tsunogai, S., S. Watanabe and T. Sato (1999). Is there a "continental shelf pump" for the absorption of atmospheric CO_2? Tellus 51B, 701-712.

Uchida, H., G.C. Johnson and K.E. Mctaggart (2010). CTD oxygen sensor calibration procedures. The GO-Ship Repeat Hydrography Manual: A collection of expert reports and guidelines, IOCCP Report No. 14, ICPO Publication Series No. 134. **Version 1, 2010:** 1-17.

Van Bleijswijk, J., R. Kempers, P. Van Der Wal, P. Westbroek, J. Egge and T. Lukk (1994). Standing stocks of PIC, POC, PON and *Emiliania huxleyi* coccospheres and liths in seawater enclosures with different phosphate loadings. Sarsia 79, 307-318.

Wakelin, S.L., J.T. Holt, J.C. Blackford, J.I. Allen, M. Butenschon and Y. Artioli (2012). Modeling the carbon fluxes of the northwest European continental

shelf: Validation and budgets. Journal of Geophysical Research 117, C05020, doi: 05010.01029/02011JC007402.
Wanninkhof, R. (1992). Relationship between wind speed and gas exchange over the ocean. Journal of Geophysical Research 97(C5), 7373-7382.
Weiss, R.F. (1974). Carbon dioxide in water and seawater: The solubility of a non-ideal gas. Marine Chemistry 2, 203-215.
Weiss, R.F. and B.A. Price (1980). Nitrous oxide solubility in water and seawater. Marine Chemistry 8, 347-359.
White, M. and P. Bowyer (1997). The shelf-edge current north-west of Ireland. Annales Geophysicae 15, 1076-1083.
Xing, J. and A.M. Davies (1996). A numerical model of the long term flow along the Malin-Hebrides shelf. Journal of Marine Systems 8, 191-218.
Xu, W., P.I. Miller, G.D. Quartly and R.D. Pingree (2015). Seasonality and interannual variability of the European Slope current from 20 years of altimeter data compared with in situ measurements. Remote Sensing of Enviornment 162, 196-207.

Table Legends

Table 1: Summary of transport fluxes for each transect. Note that the corresponding cross shelf exchanges (in Sv; = 1 x 10^6 m^3 s^{-1}) are calculated by scaling individual transport estimates to the full extent of the Hebrides Shelf edge.

Table 2: Summary of cross-shelf particulate organic silica (bSi) as weight of opal (SiO_2.0.4 H_2O), phosphorous (POP) and nitrogen (PON) fluxes for the Hebrides Shelf (~55.4 – 59.2°N) as calculated in this study.

Table 3: Summary of cross-shelf carbon fluxes for the Hebrides Shelf (~55.4 – 59.2°N) as calculated in this study. Note the change in units.

Table 4: Literature observations of the Slope Current between ~55°N and ~60°N. See also **Table 5.**

Table 5: Interannual estimates of Slope Current volume transport and depth averaged currents from selected Extended Ellett Line cruises at 57°N during October in comparison to results from this study.

Table 6: Literature estimates of offshelf exchange via the Ekman drain along the west Scotland Shelf.

Table 7: Summary offshelf fluxes of particulate material per unit area of shelf. These estimates are determined by first calculating the total offshelf flux obtained by scaling up the results of Tables 2 & 3 to the length of the shelf break studied here (516 km)

and then dividing the total flux by the area of the extended Hebrides sea region lying between 55.3°N and 59.2°N (54,747 km^2) as shown in **Figure 1**. We include the mean regional ingassing CO_2 flux for comparison.

Figure Legends

Figure 1: Map of the survey area denoting position of sampling stations.

Figure 2: Contoured surface maps (as labelled) showing regional gradients in hydrography, nutrient distributions and biogenic particulate concentrations.

Figure 3: Contoured section plots for each transect of conservative temperature, absolute salinity, density and dissolved oxygen concentration.

Figure 4: Contoured section plots for each transect of dissolved inorganic carbon (DIC), particulate organic carbon (POC), particulate organic nitrogen (PON), particulate organic phosphorus (POP), and biogenic silica (bSi).

Figure 5: Vessel Mounted Acoustic Doppler Current Profiler measurements of meridional (or zonal) current components along each transect. The position, or assumed position, of the Slope Current is indicated on each plot by the crosshairs.

Figure 6: Contoured map of air-sea CO_2 fluxes (mmol CO_2 m^{-2} d^{-1}) based on calculations described in the text. The zero flux contour is indicated by the white line.

Figure 7: Schematic showing a partial carbon budget and dominant physical circulatory features for the Hebrides Shelf in autumn 2014. Highlighted are the major carbon fluxes associated with the (offshelf) Ekman drain, (onshore) surface Ekman layer and the mean regional air-sea CO_2 as measured in this study. The mean Ekman

transports are shown in black (m^2 s^{-1}), carbon fluxes are shown in blue (units of Tg C d^{-1}) whilst mean concentrations of the carbon pools are shown in red (μmol L^{-1}).

Tables

Table 1: Summary of transport fluxes for each transect. Note that the corresponding cross shelf exchanges (in Sv; = 1 x 10^6 m^3 s^{-1}) are calculated by scaling individual transport estimates to the full extent of the Hebrides Shelf edge.

Transect	Latitude (°N)	Depth averaged current ($m\ s^{-1}$)	Slope Current Volume Transport (Sv)	Bottom Ekman Transport ($m^2\ s^{-1}$)	Cross shelf exchange (Sv)	Surface Ekman Transport ($m^2\ s^{-1}$)	Cross shelf exchange (Sv)
A	59.19	0.28	0.19[a]	1.56	0.80	1.89	0.98
C	58.22	0.15[b]	-	0.46[b]	0.24[b]	1.92	0.99
D	57.62	0.36	1.51	2.68	1.38	2.20	1.13
E	56.87	0.35	1.56	2.50	1.29	1.99	1.03
F	56.12	0.28	4[a]	1.57	0.81	2.15	1.11
G	55.37	0.19	0.53	0.74	0.38	2.07	1.07
Mean(±stdev)		0.29±0.07[b]	See Table 5	1.81±0.79[b]	0.93±0.41[b]	2.04±0.12	1.05±0.06

[a] Low confidence

[b] Depth averaged current velocities, bottom Ekman transport and cross-shelf exchange estimates along Transect C are incomplete but provided for illustrative purposes only. These results for Transect C are not used to calculate the mean values in the bottom row of the table. Note that surface Ekman transport and the corresponding surface cross shelf exchange results for Transect C are valid and are included in the calculation of the mean values.

Table 2: Summary of cross-shelf particulate organic silica (bSi) as weight of opal (SiO_2.0.4 H_2O), phosphorous (POP) and nitrogen (PON) fluxes for the Hebrides Shelf (~55.4 – 59.2°N) as calculated in this study.

	Surface Ekman Flux (onshore)			Bottom Ekman Flux (offshore)		
Transect	**bSi (kg opal m^{-1} d^{-1})**	**POP (kg P m^{-1} d^{-1})**	**PON (kg N m^{-1} d^{-1})**	**bSi (kg opal m^{-1} d^{-1})**	**POP (kg P m^{-1} d^{-1})**	**PON (kg N m^{-1} d^{-1})**
A	2.21	0.21	1.28	2.84	0.18	1.06
C	3.66	0.24	1.58	0.97	0.04	0.75
D	4.96	0.26	1.81	3.90	0.17	1.31
E	2.70	0.23	1.76	4.32	0.18	1.47
F	3.24	0.28	2.05	2.25	0.06	2.49
G	4.33	0.16	1.51	1.19	0.02	0.28
Mean (±stdev)	3.52 (1.02)	0.23 (0.04)	1.66 (0.27)	2.90 (1.26)	0.12 (0.07)	1.32 (0.80)

Table 3: Summary of cross-shelf carbon fluxes for the Hebrides Shelf (~55.4 – 59.2°N) as calculated in this study. Note the change in units.

	Surface Ekman Flux (onshore)[a]							Bottom Ekman Flux (offshore)[b]							
Transect	**DIC (tonnes C m^{-1} d^{-1})**	**POC (kg C m^{-1} d^{-1})**	**PIC (g C m^{-1} d^{-1})**	**DOC (tonnes C m^{-1} d^{-1})**	**Total (tonnes C m^{-1} d^{-1})**	**%Org (%)**	**%Inorg (%)**	**DIC (tonnes C m^{-1} d^{-1})**	**POC (kg C m^{-1} d^{-1})**	**PIC (g C m^{-1} d^{-1})**	**DOC (tonnes C m^{-1} d^{-1})**	**Total (tonnes C m^{-1} d^{-1})**	**%Org (%)**	**%Inorg (%)**	**DICxs (kg C m^{-1} d^{-1})**
A	4.05	12.07	11.20	0.12	4.18	3.27	96.73	3.41	9.52		0.22	3.64	6.31	93.69	31.56
C	4.11	12.22	169.83	0.13	4.25	3.25	96.75	1.01	4.25		0.06	1.08	6.41	93.59	9.31
D	4.69	12.09	21.06	0.14	4.84	3.23	96.77	5.85	11.05		0.38	6.24	6.24	93.76	54.22
E	4.26	14.93	135.05	0.13	4.40	3.31	96.69	5.44	12.14	1119.67	0.35	5.80	6.29	93.71	50.58
F	4.57	17.12	66.77	0.14	4.73	3.34	96.66	3.42	28.37		0.22	3.67	6.82	93.18	31.76
G	4.42	12.17		0.14	4.57	3.25	96.75	1.61	2.66	79.67	0.10	1.71	6.25	93.75	14.97
Mean (±stdev)	4.35 (0.26)	13.43 (2.13)	80.78 (69.79)	0.13 (0.01)	4.50 (0.26)	3.28 (0.043)	96.72 (0.004)	3.94 (1.72)	12.75 (9.48)	599.7 (735.4)	0.26 (0.11)	4.21 (1.84)	6.38 (0.244)	93.62 (0.244)	36.62 (15.99)

[a] The Surface Ekman Flux is not affected by the patchy ADCP sampling and results from Transect C are used in the calculation of mean surface fluxes presented in the last row of the table.

[b] Bottom Ekman Flux estimates (the "Ekman Drain") along Transect C are incomplete but provided for illustrative purposes only. Results from Transect C are not used to calculate the mean bottom fluxes in the last row of the table.

Table 4: Literature observations of the Slope Current between ~55°N and ~60°N. See also **Table 5.**

Latitude (°N)	Slope Current velocity (m s^{-1})	Slope Current volume transport (Sv)	Notes	Reference
59	0.3	1.7	Mean current	Huthnance (1986)
58	0.15	1.5		
56	0.06	-		
57.1	0.16	0.5	Current meter	Booth and Ellett (1983)
60.22	0.77	-	Current meter (maximum hourly mean)	Carter *et a*l., (1987)
60.21	0.62	-		
60.17	0.87	-		
59.78	0.78	-		
59.66	0.81	-		
59.14	0.52	-		
59.09	0.78	-		
58.14	0.47	-		
58.11	0.56	-		
58.01	0.50	-		
57.94	0.66	-		
57.35	0.52	-		
57.31	0.46	-		
56.6	-	1.6	Model estimate	Holt *et al.,* (2009)
60	0.30	-		Huthnance and Gould (1989)
54.5	0.10	-	Current meter	White and Bowyer (1997)
55.04	0.22	-	Current meter	
56.48	0.15	2	ADCP mooring	Souza *et al.,* (2001)
59.5	-	1.7	VMADCP	Chafik *et al.,* (2014)
57	-	1.8	Geostrophy	Holliday et al., (2015)

Table 5: Interannual estimates of Slope Current volume transport and depth averaged currents from selected Extended Ellett Line cruises at 57°N during October in comparison to results from this study

Cruise Identifier	D223	CD176	D312	DY017 (this study)
Date	Oct 1996	Oct 2005	Oct 2006	Oct-Nov 2014
Latitude (°N)	57.06°N	56.8°N	57°N	55.4 – 57.6°N[a]
Max VMADCP depth penetration (m)	400	275	350	400
Current width (km)	37	76	19	35-57
Depth avg current (m s^{-1})	0.3	0.50	0.16	0.19-0.36
Volume transport (Sv)	1.06	1.48	0.53	0.53 – 1.56[b]

[a] Note that these summary values do not include information from Transects A or C of the present study due to limitations within the data on these transects.

[b] Volume transport estimate of 4 Sv obtained from Transect F of the present study (Table 1) excluded due to the distorting influence of a cyclonic eddy on this transect.

Table 6: Literature estimates of offshelf exchange via the Ekman Drain along the west Scotland Shelf.

Latitude (°N) / region	Transport ($m^2 s^{-1}$)	Volume Transport (Sv)	Reference
54-57°N	1.75	~0.6	Holt and Proctor (2008)
~53-63°N	-	0.13 – 0.28	Holt et al., (2009)
56.48°N	1.6	0.83	Simpson and McCandliss (2013)
56.48°N	0.46	0.3	Souza et al., (2001)
W. Scotland Shelf	-	~0.52	Huthnance *et al*., (2009)
Western shelf ~52-60°N	-	1.15	Wakelin *et al*., (2012)
Hebrides Shelf ~55-59°N	1.81	0.93	This Study

Table 7: Summary offshelf fluxes of particulate material per unit area of shelf. These estimates are determined by first calculating the total offshelf flux obtained by scaling up the results of Tables 2 & 3 to the length of the shelf break studied here (516 km) and then dividing the total flux by the area of the extended Hebrides sea region lying between 55.3°N and 59.2°N (54,747 km^2) as shown in **Figure 1**. We include the mean regional ingassing CO_2 flux for comparison.

Transect	POC (mmol C m^{-2} d^{-1})	PON (mmol N m^{-2} d^{-1})	POP (mmol P m^{-2} d^{-1})	PIC (mmol C m^{-2} d^{-1})	bSi-opal (mmol opal m^{-2} d^{-1})	CO_2 flux (mmol C m^{-2} d^{-1})
A	7.48	0.71	0.05		0.40	
C	3.34	0.50	0.01		0.14	
D	8.68	0.88	0.05		0.55	
E	9.54	0.99	0.05	0.88	0.60	
F	22.28	1.68	0.02		0.31	
G	2.09	0.19	0.01	0.06	0.17	
Mean (±stdev)	10.01 (7.44)	0.89 (0.54)	0.04 (0.02)	0.47 (0.58)	0.41 (0.18)	-3.2

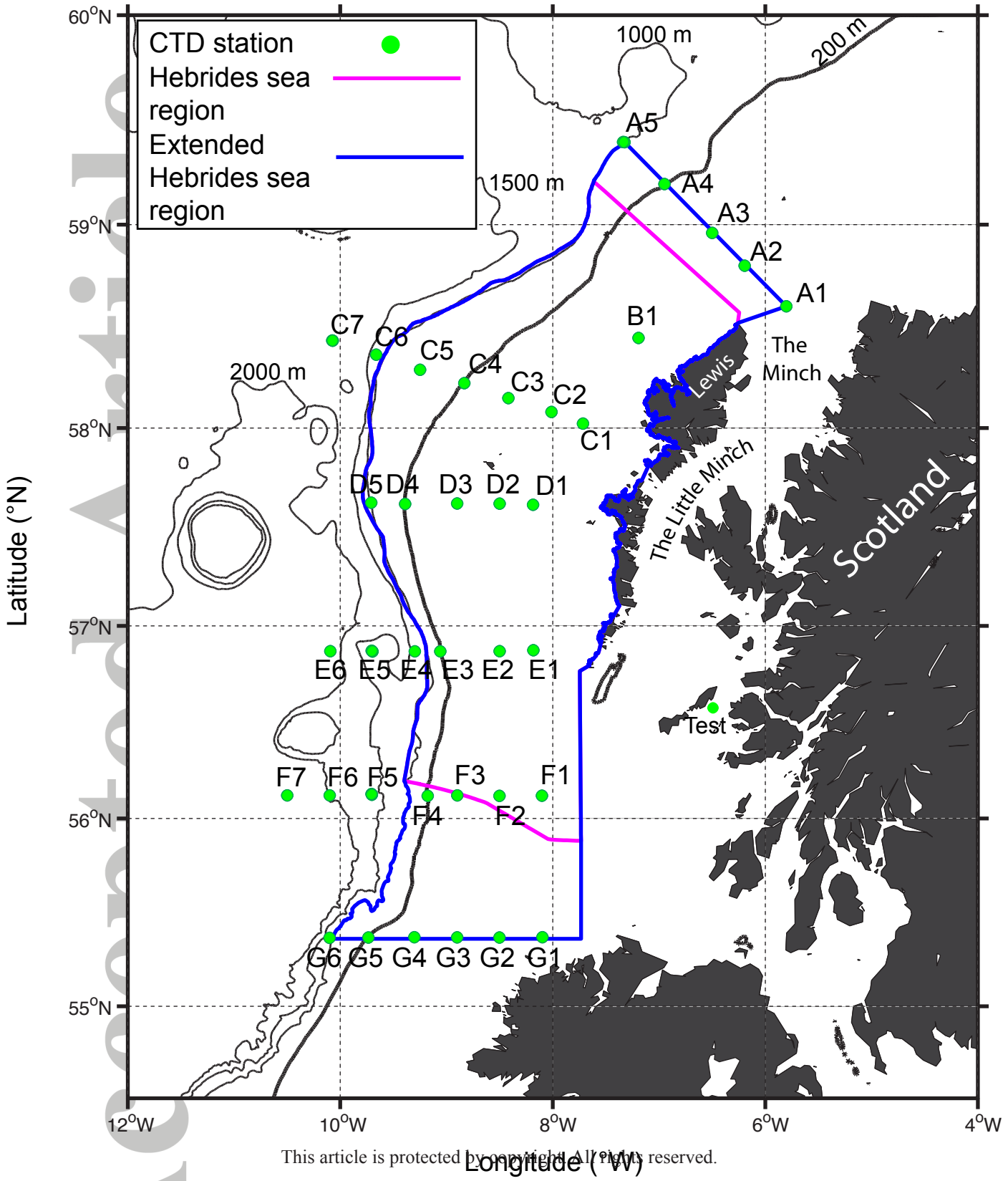

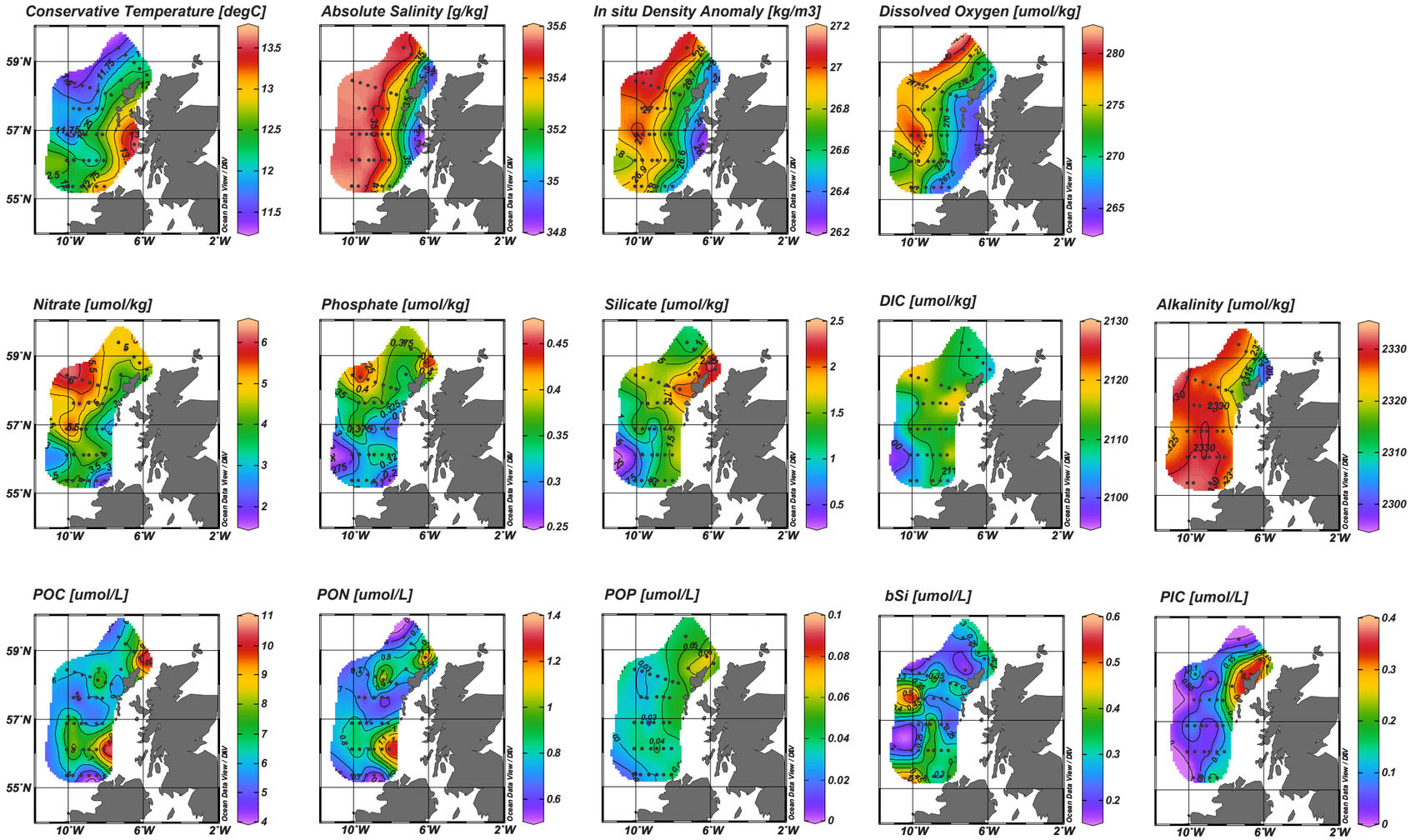

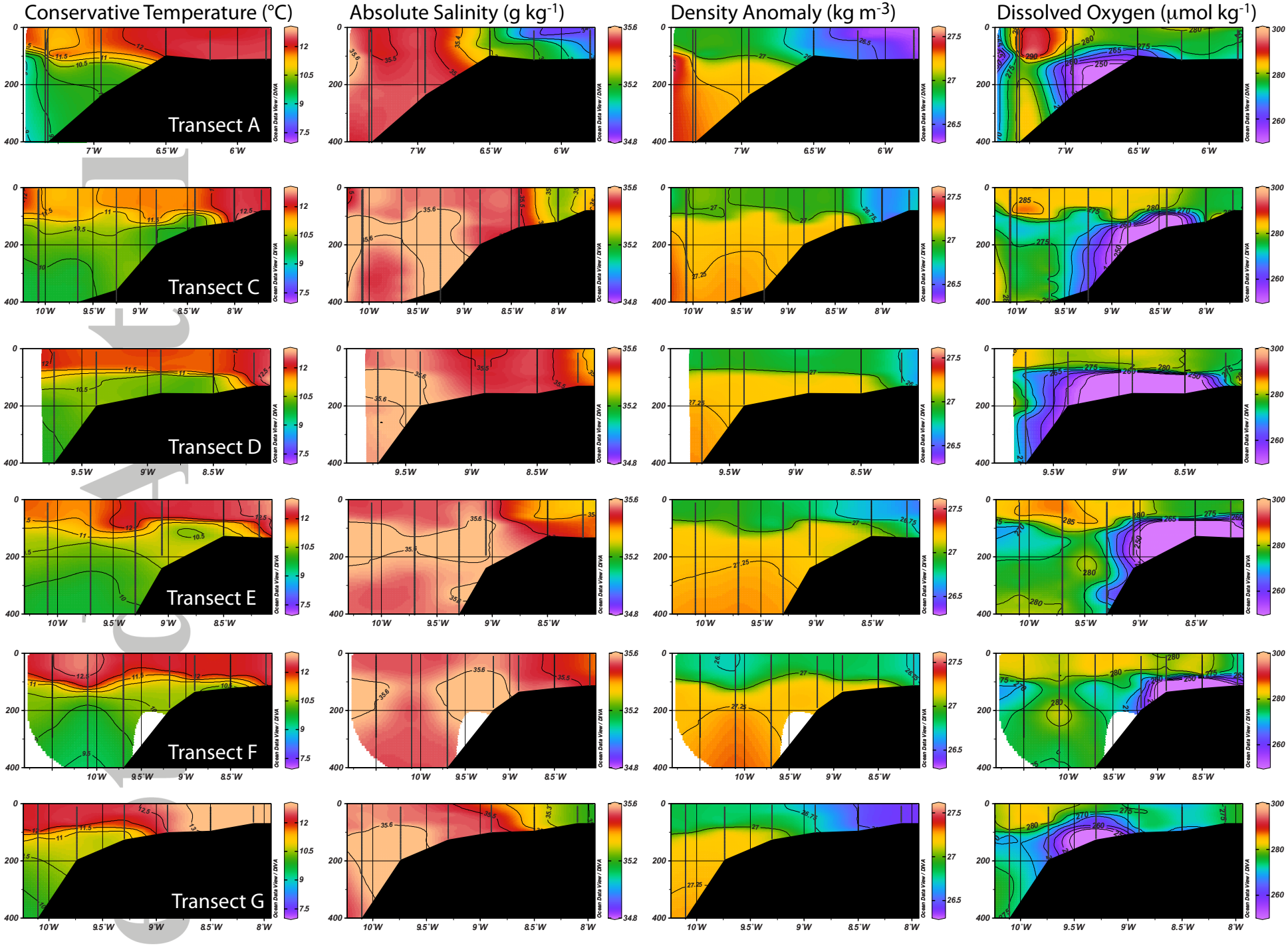

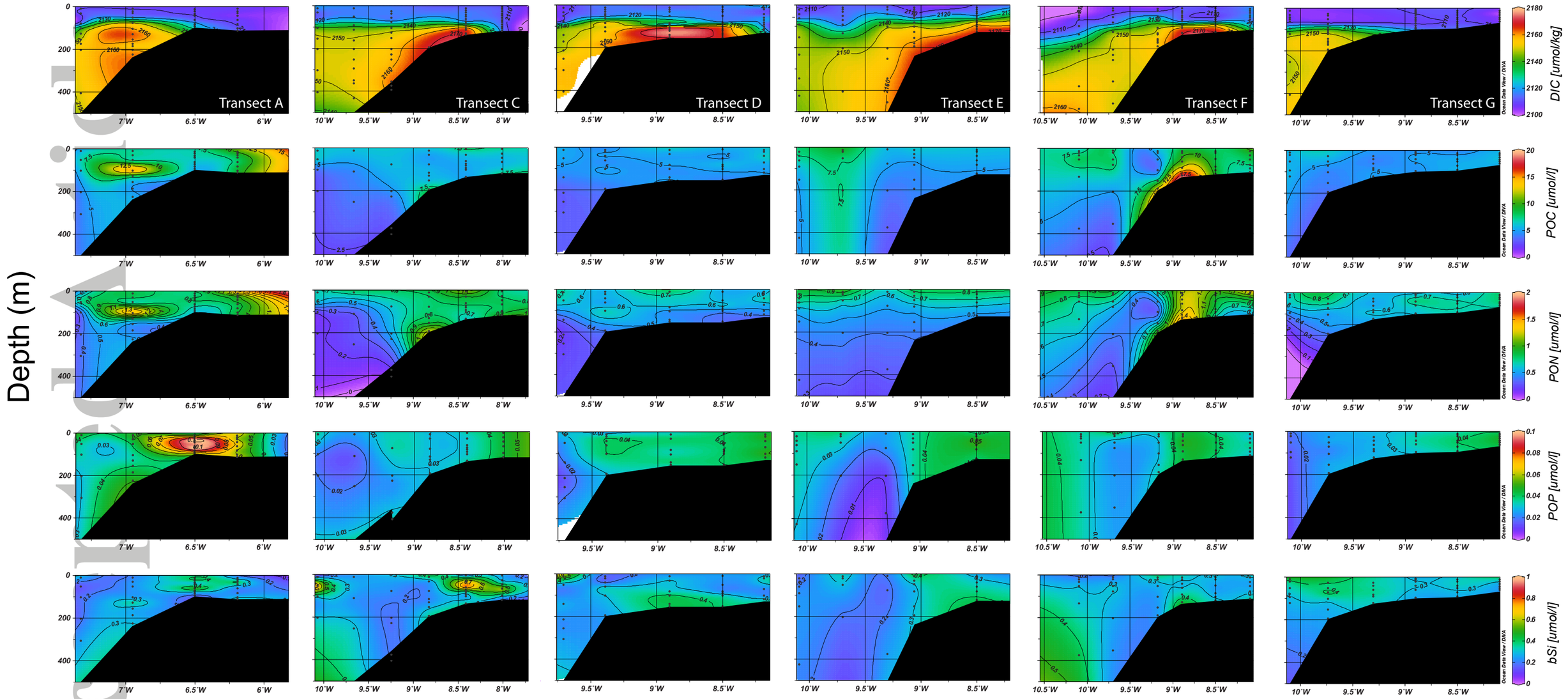

Transect A

Transect C

Transect D

Transect E

Transect F

Transect G

?

?

0
200
400

–7.2
–7
–6.8
–6.6
–6.4
–6.2
–10
–9.5
–9
–8.5
–8

Depth (m)

Longitude (°W)

East-west current velocity (cm/s) (same scale)

60
40
20
0
–20
–40
–60

North-south current velocity (cm/s)